Dalton Transactions

ROYAL SOCIETY OF CHEMISTRY

PERSPECTIVE

View Article Online
View Journal

Cite this: DOI: 10.1039/d6dt00351f

Recent development in iron- and manganese-catalysed hydrosilylation: unravelling diverse structures of complexes and mechanisms

Muhammad Younus † and Kouki Matsubara *

Received 10th February 2026,
Accepted 13th April 2026

DOI: 10.1039/d6dt00351f

rsc.li/dalton

The emerging field of organometallic catalysis has turned toward first-row transition metals due to their greater abundance, lower cost, and unique reactivity profiles. Among these, iron and manganese, as the most abundant transition metals in the Earth's crust, have emerged as promising alternatives to precious metals in catalytic applications. Over the past half-decade, (2019 to present), there has been significant progress in Fe- and Mn-catalysed hydrosilylation reactions involving unsaturated bonds such as C=C, C≡C, C=O, and C≡N. This perspective provides a comprehensive summary of recent developments in the hydrosilylation of alkenes, alkynes, carbonyl compounds, and nitrogen-containing substrates, catalysed by various well-defined Fe and Mn complexes. It highlights not only the synthetic scope of these transformations but also the mechanistic insights that govern their reactivity. Particular emphasis is placed on the impact of ligands (P-, N-, and C-donors) on catalytic performance, as well as comparisons with structurally related polydentate ligand systems. The analysis further explores how variations in ligand architecture influence both catalytic activity and selectivity. This perspective ultimately aims to provide valuable guidance for future catalyst and ligand design, thereby advancing sustainable and efficient catalytic processes using base metals.

1. Introduction

Iron is the most abundant transition metal in the Earth's crust, while manganese is the third most abundant transition metal. Both metals have been widely employed in catalysis, including organic transformations and energy-storage technologies, contributing to the advancement of green and sustainable chemistry as key earth-abundant metals.[1,2] Their high natural abundance, low toxicity, and diverse redox properties make them attractive alternatives to precious transition metals. Homogeneous catalysts enable reactions to proceed under relatively mild conditions while achieving high chemo-, regio-, and stereoselectivity and are therefore widely employed in small- and medium-scale syntheses, such as those used in the production of fine chemicals.[3,4] Over the past several years, interest in the use of Fe- and Mn-based catalysts for homogeneous organic transformations has increased significantly.[5,6] Iron catalysts have been extensively explored for a variety of reactions, including cross-coupling, C–H activation, and hydrofunctionalization, providing sustainable alternatives to noble metals such as Rh, Pd, Pt, Ir and Ru.[7,8] Manganese, owing to its versatile oxidation states, has also emerged as a promising catalyst for oxidation reactions, hydrogenation, and radical transformations, enabling selective and efficient chemical processes.[9,10] These developments highlight the growing importance of iron and manganese in advancing sustainable catalytic methodologies while maintaining high catalytic performance in modern organic synthesis.[11–14]

The catalytic reduction of functional groups is an essential transformation in the production of fine chemicals in both laboratory and industrial settings.[15] A major advantage of catalytic reduction processes is their ability to combine effective reducing power with relatively mild and controlled reaction conditions. Consequently, numerous catalytic methods have been developed for the reduction of a wide range of functional groups. Traditionally, such reductions often rely on stoichiometric amounts of reactive metal hydrides, such as $NaBH_4$ and $LiAlH_4$, which generate significant quantities of metal-containing waste.[16,17] As a result, the sustainability and atom economy of these approaches are often unfavourable.[17,18] In contrast, catalytic hydrogenation using molecular hydrogen has attracted considerable attention from both economic and environmental perspectives; however, it often requires catalysts based on scarce noble metals, high hydrogen pressures, and demanding reaction conditions. Iron catalysts have also demonstrated remarkable activity in classical homogeneous catalytic transformations, such as hydrogenation and hydroformylation. In recent years, well-defined Fe complexes have been

Department of Chemistry, Fukuoka University, 8-19-1 Nanakuma, Fukuoka 814-0180, Japan. E-mail: kmatsuba@fukuoka-u.ac.jp
† M. Younus and K. Matsubara equally contributed to this study.

reported to efficiently catalyse the hydrogenation of alkenes, ketones and imines, as well as hydroformylation processes, highlighting their versatility as sustainable alternatives to precious-metal systems.[7,8,19]

Hydrosilylation reactions, which employ hydrosilanes as mild hydride sources, provide an attractive alternative for the reduction of a wide range of functional groups. These transformations enable the reduction of substrates such as alkenes, alkynes, aldehydes, ketones, carboxylic acids, esters, amides, imines and nitriles under comparatively mild conditions.[20–22] Because hydrosilanes are generally stable, readily available and relatively easy to handle, catalytic hydrosilylation has emerged as a valuable alternative to conventional hydrogenation-based reduction methods.[23] Under appropriate catalytic conditions, hydrosilanes can be activated to generate silylated intermediates or reduced products efficiently.[24] Moreover, the resulting organosilicon compounds are valuable synthetic intermediates that can be further transformed into functional materials and complex molecular architectures.[25,26]

Several precious transition metals, such as Rh, Pt, Pd, Ir, and Ru, have been widely employed in hydrosilylation catalysis and are recognised as highly active systems for the reduction of numerous functional groups.[18,27,28] These metals have dominated the field since the first report of hydrosilylation in 1947.[29] Platinum-based catalysts, including Speier's catalyst ($H_2PtCl_6{\cdot}6H_2O$ in iPrOH)[30] and Karstedt's catalyst, are extensively used for the synthesis of organosilicon compounds from alkenes in both laboratory and industrial settings.[31] However, the high cost, limited availability, and potential toxicity of these noble metals have driven the development of catalytic systems based on earth-abundant alternatives.[32] Consequently, the replacement of precious metals with first-row transition metals such as Fe and Mn has attracted considerable attention in recent years.[33,34] Fe- and Mn-catalysed hydrosilylation reactions meet several key requirements for sustainable reduction processes, enabling the synthesis of valuable organic molecules under milder and more environmentally benign conditions.[35,36] In addition, 3d transition metals exhibit diverse coordination environments, spin states, and geometries, which can facilitate catalytic activity through favourable electronic configurations.[37] These characteristics provide opportunities for the development of catalytic systems with distinct reactivity and selectivity, offering viable alternatives to traditional noble-metal catalysts.[38]

This Perspective highlights recent advances in Fe- and Mn-catalysed hydrosilylation reactions reported since 2019.[22] Particular emphasis is placed on the structural features of catalytically active complexes, their applications in hydrosilylative reductions, and on mechanistic insights obtained from both experimental and computational studies.

2. Hydrosilylation by iron complexes

Iron complexes have attracted increasing attention as active catalysts for hydrosilylation reactions in recent years, primarily driven by the development of efficient catalytic systems based on earth-abundant metals.[32,39] The early evolution of Fe-catalysed hydrosilylation reactions reported before 2018 is briefly summarised below.

The first application of an Fe complex **A** in catalytic hydrosilylation was reported by Brunner in the 1970s (Fig. 1), demonstrating that Fe catalysts could promote the hydrosilylation of carbonyl compounds without the formation of dehydrogenative by-products.[40,41]

Despite this early contribution, Fe-catalysed hydrosilylation received limited attention for several decades, with renewed interest emerging only later as efforts shifted toward the development of catalysts based on readily available and inexpensive transition metals. As a result of this renewed focus, a range of Fe complexes capable of efficiently catalysing hydrosilylation reactions was subsequently reported.[41] In 2012, Nakazawa and co-workers reported an Fe(II) terpyridine complex **B** (Fig. 1) that exhibited high catalytic activity and selectivity in the hydrosilylation of alkenes upon activation with $NaEt_3BH$.[42] Shortly thereafter, Sortais and Darcel developed well-defined $CpFe(CO)_2(L)$ complexes (**C**) (L = PCy_3 or NHC) (Fig. 1), which efficiently catalysed the hydrosilylation of esters, aldimines, and ketimines under mild conditions, with activation achieved through visible light irradiation.[43,44]

In 2013, Zhuo and Beller introduced an Fe-catalysed protocol for the reduction of carboxylic acid esters to alcohols using a $Fe(stearate)_2/NH_2NH_2$ system, establishing a practical and sustainable strategy for ester hydrosilylation.[45] Ligand development further expanded the scope of Fe catalysis. Walter and Huang designed phosphinite–iminopyridine (PNN) Fe complexes **D** (Fig. 1) that promoted anti-Markovnikov hydrosilylation of alkenes with excellent functional-group tolerance.[46]

Beyond alkene and carbonyl reductions, Fe catalysts were also applied to reductive functionalisation reactions. In 2014, Cantat and co-workers reported Fe(II) phosphine-supported systems capable of promoting CO_2 reduction with hydrosilanes

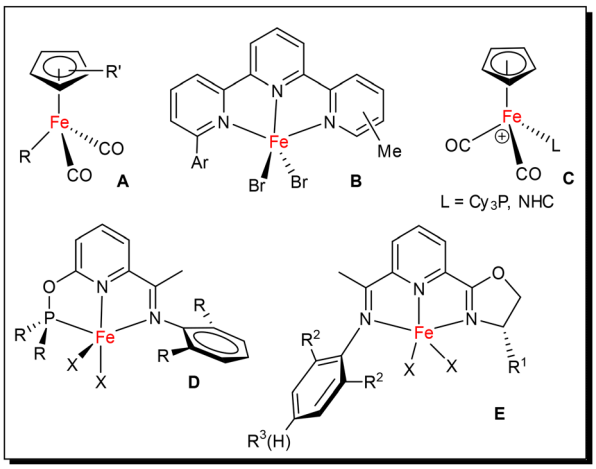

Fig. 1 Iron complexes **A–E** used for hydrosilylation in reports earlier than 2018.

to formamide and methylamine derivatives under mild conditions.[47] In a related study, Sortais and Darcel described an Fe(0)-catalysed cascade synthesis of *N*-alkylated anilines under hydrosilylation conditions using $Fe(cod)(CO)_3$ as a visible-light-activated precatalyst.[48]

The development of enantioselective Fe-catalysed hydrosilylation soon followed. Huang and co-workers reported chiral iminopyridine–oxazoline (IPO) Fe complexes **E** (Fig. 1) that enabled asymmetric hydrosilylation of aryl ketones with excellent yields and enantioselectivities (up to 93% ee).[49] Similarly, Lu and co-workers achieved highly regio- and enantioselective anti-Markovnikov hydrosilylation of 1,1-disubstituted aryl alkenes using related ligand frameworks.[50]

In 2016, Gade and co-workers conducted a comprehensive mechanistic investigation that clarified the activation pathways of Fe carboxylate precatalysts and the reaction mechanisms of the active species in ketone hydrosilylation (Fig. 2). Their study demonstrated that Fe(II) complexes bearing bis(imino)pyridine ligands activate the Si–H bond of hydrosilanes *via* σ-bond metathesis rather than oxidative addition, thereby providing important mechanistic insight into Fe-catalysed hydrosilylation.[51] In a complementary study, Findlater and co-workers reported that well-defined Fe(0) complexes **F** (Fig. 3) efficiently catalysed the reduction of aldehydes and ketones under solvent-free conditions with broad functional group tolerance, highlighting the versatility of low-valent Fe species in hydrosilylation chemistry.[52] Collectively, these studies establish key mechanistic paradigms and demonstrate the diversity reactivity of iron catalysts in hydrosilylation, which directly relates to the catalytic systems discussed in this review.

In early 2018, Zhu and co-workers introduced Fe complex **G** bearing 2,9-diaryl-1,10-phenanthroline ligands (Fig. 3), which exhibited distinctive reactivity and high regioselectivity in the hydrosilylation of alkenes.[53] In the same year, Findlater and co-workers introduced a distinct Fe complex **F** for the hydrosilylation of imines, enabling their efficient conversion into secondary amines under mild conditions.[54] Fernandez and co-workers developed an Fe complex **H** supported by an anthraquinoid ligand (Fig. 3), which effectively catalysed the hydrosilylation of aldehydes and ketones at room temperature (Scheme 7). This catalyst exhibited broad functional-group tolerance and high turnover frequencies, even under solvent-free conditions.[55] Later on, Lu and co-workers introduced a novel Fe-catalysed method, achieving highly Markovnikov-selective and enantio-selective hydrosilylation of aliphatic terminal olefins, providing access to valuable chiral organosilicon compounds.[56] Collectively, these studies establish iron as a versatile and mechanistically diverse platform for hydrosilylation chemistry, forming the foundation for the developments discussed in this review.

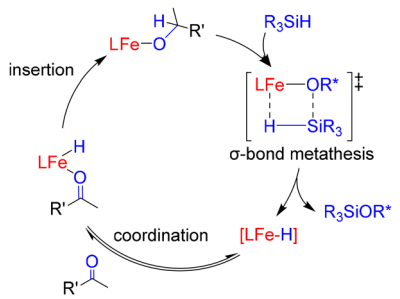

Fig. 2 Proposed mechanism for hydrosilylation of ketones using Fe carboxylate precatalyst.

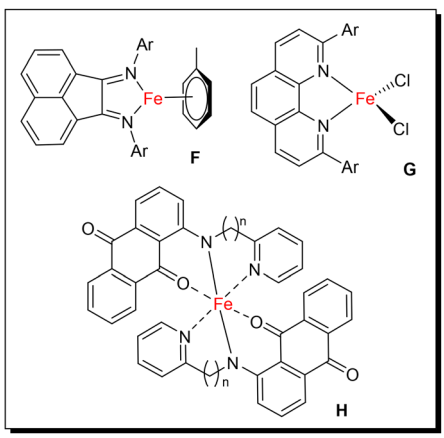

Fig. 3 Iron complexes **F–H** used for hydrosilylation in reports earlier than 2018.

2.1 Hydrosilylation of alkanes, alkenes, and alkynes

In 2019, Zhu and co-workers reported Fe complex **1**, bearing a 2,9-diaryl-1,10-phenanthroline ligand, for the double hydrosilylation of alkynes in the presence of EtMgBr, enabling efficient access to geminal bis(silanes), which are versatile synthetic intermediates (Scheme 1). Complex **1** was found to outperform other metal-based systems, offering complete atom economy, excellent regioselectivity, and mild reaction conditions. The phenanthroline ligand facilitated the generation of an active low-valent Fe species, which promoted two successive hydrosilylation steps: initial formation of β-(*E*)-vinylsilanes, followed by a second hydrosilylation to afford geminal bis(silanes). Comparative studies with alternative ligands, including tridentate pyridine–diamine systems, revealed that

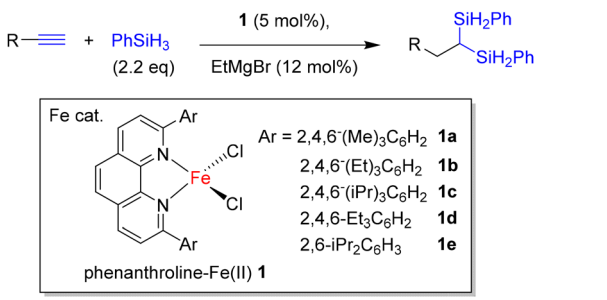

Scheme 1 The synthesis of geminal bis(silanes) by double hydrosilylation of alkynes.

variations in the ligand environment had a pronounced impact on regioselectivity.[57]

The plausible mechanistic elucidation begins with the activation of complex **1**. The key step determining regioselectivity was the migration of hydrogen from an intermediate **Int-1** to **Int-2** *via* a transition state **TS-1** (Fig. 4). This selectivity was primarily influenced by the α-silicon effect in the vinylsilane intermediate. Due to the lower electronegativity of silicon compared to carbon, the β-position of the vinylsilane exhibits lower electron density than the α-position of **TS-2**. As a result, the Fe-bound hydride preferentially attacked on the β-position, leading to the formation of a geminal bis(silane) product. Supporting this mechanistic proposal, density functional theory (DFT) calculations indicated that the energy barrier for the α-selective pathway is 6.9 kcal mol^{-1} lower than that for the β-selective pathway, favouring the observed product distribution.[57]

Ligand-controlled, highly active regiodivergent hydrosilylation of alkynes was reported by Zhu and co-workers in 2020. The Fe complexes **1c** and **1f**, which differ only in the aryl substituents on the phenanthroline scaffold, dictated the regioselectivity by tuning the steric and electronic environment around the metal centre. Specifically, complex **1c**, bearing 2,4,6-triisopropylphenyl substituents, favoured anti-Markovnikov addition, whereas **1f**, featuring 3,5-disubstituted aryl groups, enhanced Markovnikov selectivity (Scheme 2). X-ray crystallographic analyses confirmed the steric bulk and spatial orientation of the ligands, which influenced the approach of the alkyne to the Fe centre by stabilising the transition states through non-covalent interactions, such as π–π stacking. This ligand-controlled strategy delivered high turnover numbers (up to 35 500 h^{-1}) together with excellent regioselectivity.[58]

In 2024, Zhu and co-workers further elucidated the reaction mechanism using complex **1**, which they termed spin-delocalisation-regulated reactivity (SDRR). The reaction begins with the *in situ* reduction of the Fe(II) pre-catalyst by EtMgBr to generate a formal Fe(0) species, which subsequently coordinates to the alkyne and silane to form intermediate **Int-2**. Ligand-to-ligand hydrogen transfer (LLHT) from phenylsilane to the C≡C triple bond then occurs *via* transition state **TS-1**, affording **Int-3**. Intermediate **Int-3** subsequently undergoes reductive elimination through **TS-2** to yield **Int-4**. Finally, substrate exchange of **Int-4** with a fresh alkyne and silane releases the hydrosilylation product and regenerates **Int-2**, thereby completing the catalytic cycle (Fig. 5). Importantly, they demonstrated that spin delocalisation over the redox-active 1,10-phenanthroline ligand enables regulation of both the spin and oxidation states of the open-shell Fe centre, which is essential for efficient catalysis. A spin crossover between the triplet and quintet states was observed during the reaction: oxidative addition step was favoured on the triplet Fe surface, whereas reductive elimination was facilitated by the quintet state.[59]

In the same year, the Zhu group reported 1,10-phenanthroline-based open-shell Fe complexes **1** that exploit spin-state dynamics to enable allylic C(sp^3)–H silylation (Scheme 3). In

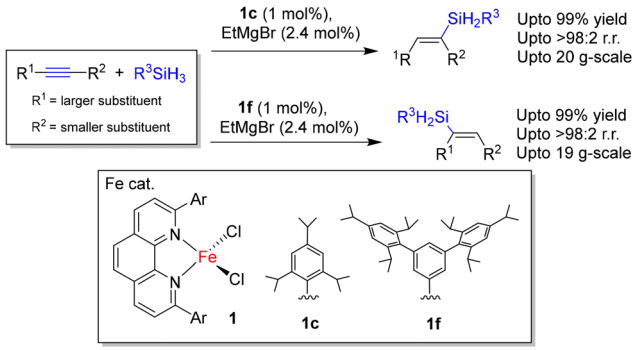

Scheme 2 Fe-catalysed regiodivergent hydrosilylation of alkynes.

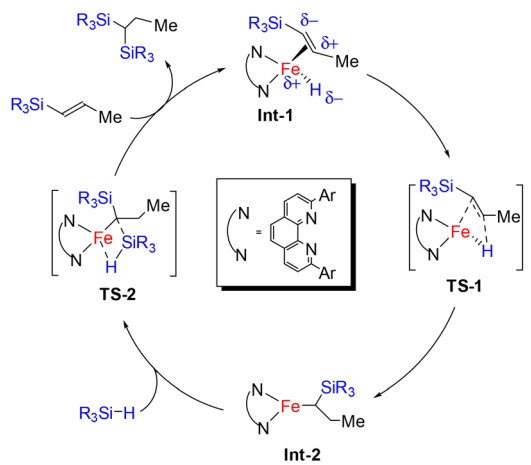

Fig. 4 Proposed mechanism for the Fe-catalysed double hydrosilylation of alkynes by using complex **1**.

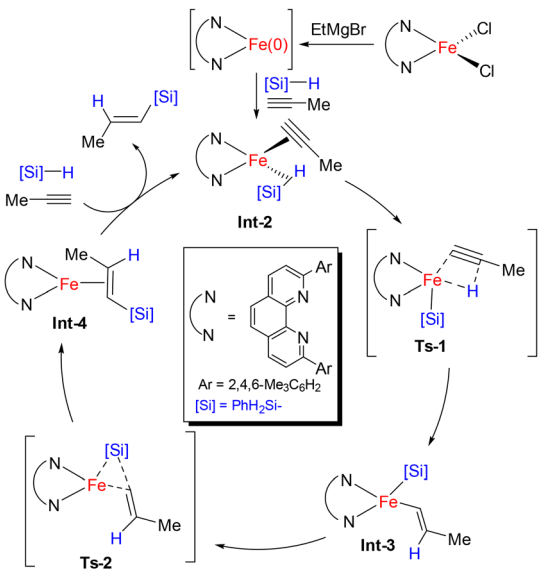

Fig. 5 Proposed catalytic cycle for regiodivergent hydrosilylation of alkyne.

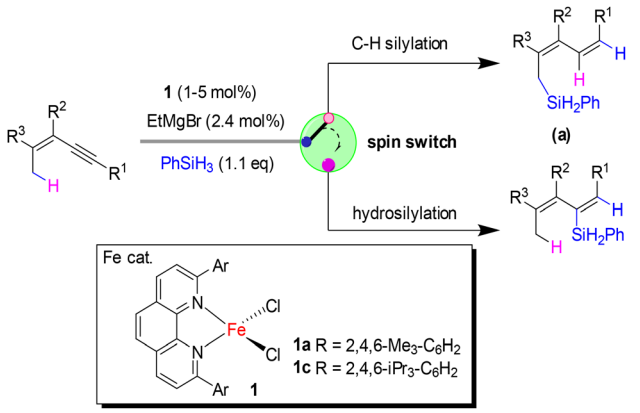

Scheme 3 Fe-catalysed formal hydrosilylation of 1,3-enynes by using complex **1**.

this system, spin crossover at the Fe centre promotes conventional alkyne hydrosilylation, whereas conservation of the spin state diverts the reaction pathway towards a distinct allylic C–H silylation process. Notably, this transformation is accompanied by the formal hydrogenation of the alkyne moiety, as both C–H transfer from the allylic carbon and Si–H transfer from hydrosilane occur, ultimately affording allylsilane products. Unlike classical ligand-assisted mechanisms, this reaction proceeds *via* a substrate-assisted C–H activation pathway, in which the silyl group derived from the hydrosilane directly participates in C–H bond cleavage and is incorporated into the final product. Density functional theory (DFT) calculations combined with isotope-labelling experiments confirmed that the electronic structure of the Fe–phenanthroline complex is central to the observed catalytic activity and that ligand-to-ligand hydrogen transfer (LLHT) plays a crucial role in facilitating product formation.[60]

In the next year, Hong and Lu (2020) investigated an Fe-catalysed asymmetric hydrosilylation of vinylcyclopropanes (VCPs) *via* stereospecific C–C bond cleavage using phenylsilane ($PhSiH_3$). Using Fe complex **2** bearing a tridentate chiral NNN ligand, this methodology afforded chiral allylic silanes with high anti-Markovnikov selectivity (Scheme 4). The observed anti-Markovnikov selectivity can be rationalised by the preferential insertion of the olefin into the Fe–H bond at the less

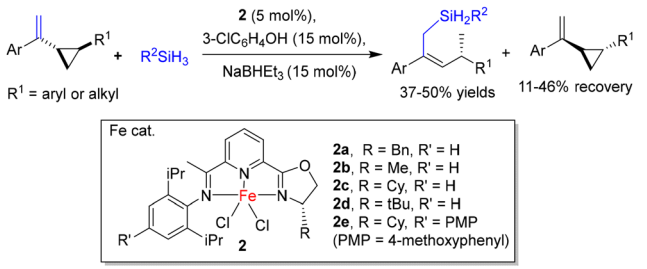

Scheme 4 Hydrosilylation of VCPs with high enantioselectivity *via* C–C bond cleavage.

substituted carbon centre, which is favoured due to steric and electronic factors associated with the Fe–H intermediate. These products serve as valuable intermediates in organic synthesis, enabling the construction of structurally complex molecules. Furthermore, this approach enables the kinetic resolution of racemic VCPs, providing access to enantioenriched substrates that are otherwise difficult to synthesise, with moderate to excellent enantioselectivity. Reaction temperatures ranging from room temperature to 80 °C efficiently promoted selective C–C bond cleavage, leading to the formation of enantioenriched allylic silanes with excellent regio- and stereocontrol.[61]

They performed a mechanistic study of the Fe-catalysed asymmetric hydrosilylation of VCPs by combining computational and experimental studies, offering a thorough understanding of the stereospecific C–C bond cleavage pathway.[61] *In situ* activation of complex 2 by a hydride source in the presence of $PhSiH_3$ initiates the catalytic cycle, producing an active Fe-silyl species (**Int-1**). This intermediate undergoes migratory insertion of the C=C bond into the Fe–Si bond in an anti-Markovnikov fashion. The resulting Fe intermediate (**Int-2**) then promotes ring opening through stereospecific β-carbon elimination to form **Int-3**. This step proceeds *via* a radical- or carbocation-like transition state, ultimately delivering the *Z*-allylic silane product with high enantiomeric purity (Fig. 6). The Fe catalyst successfully distinguishes between the two enantiomers in reactions using racemic VCPs, converting one while leaving the other enantioenriched, consistent with a kinetic resolution mechanism.

Tilley and co-workers in 2020, explored Fe complex FeCp*($PiPr_2Me$)N_2 (**3a**, Cp* = pentamethylcyclopentadienyl), which was *in situ* converted into the catalytically active cationic species [FeCp*($PiPr_2Me$)SiH_3R][BArF] (**3b**, BArF = tetrakis(3,5-bis(trifluoromethyl)phenyl)borate) upon treatment with $PhSiH_3$ and [Ph_3C][BArF]. Ligand modulation played a decisive role in tuning the electronic and steric properties of the Fe centre, thereby governing the catalytic efficiency in the hydrosilylation of terminal alkenes and internal alkynes with

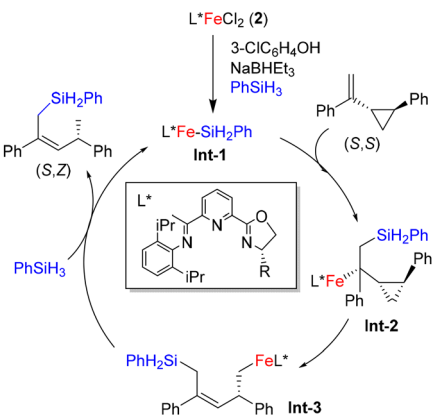

Fig. 6 Proposed mechanism for asymmetric hydrosilylation of vinylcyclopropane by an iron complex **2**.

primary silanes (Scheme 5). The phosphine ligand framework stabilised the Fe core, suppressed catalyst deactivation, and enabled controlled activation of both silane and the alkene or alkyne substrates. Increased electron density at the Fe centre facilitated Si–H bond activation, resulting in enhanced catalytic activity. Notably, hydrosilylation of internal alkynes proceeded with high *cis*-selectivity, affording the corresponding *Z*-vinylsilanes selectively.[62]

The reaction mechanism using complex **3a** was thoroughly elucidated, revealing an efficient and highly selective pathway for Si–H addition to alkenes using primary silanes.[62] Central to this reactivity is the *in situ* generation of the cationic species **3b**, which activates Si–H bonds through a weak cooperative interaction at the Fe centre. As illustrated in Fig. 7, activation of the Si–H bond can proceed through different coordination modes, **A–C**. Initially, the silane interacts with the Fe centre to form a moderately bound η^2-silane complex **A**. Stronger activation leads to Si–H bond cleavage and the formation of reactive silylene–dihydride intermediates (**B** and **C**) *via* double oxidative addition.[63,64] The catalytic process then proceeds through Si–C bond formation in which the activated Si–H unit adds across the C=C bond of the alkene, generating the corresponding alkylsilane product with high regioselectivity. Notably, this transformation proceeds without classical electron transfer at the metal centre, distinguishing it from the traditional Chalk–Harrod mechanism.[65–67]

In 2020, Kamitani and co-workers reported a series of PNN pincer-type Fe complexes **4** for the hydrosilylation of alkenes (Scheme 6). This study was notable because the steric properties of the ligands strongly influenced catalytic activity, which was quantitatively described using the percent buried volume (%V_{Bur}). The analysis revealed a hemisphere- and distance-dependent steric environment, demonstrating that the spatial arrangement of the ligand significantly affects the reactivity of the Fe centre, and that steric hindrance plays a crucial role in regulating catalytic efficiency.[68]

The mechanistic study of hydrosilylation catalysed by the PNN pincer-type Fe complex **4**, bearing ligands with varied substituents, highlighted the crucial influence of ligand sterics on reactivity. A modified Chalk–Harrod mechanism, involving alkene insertion into the Fe–Si bond, was proposed (Fig. 8).[18] In earlier work, the initially activated dihydride complex **A** was characterised experimentally.[69] Coordination of an alkene to **A**, accompanied by H_2 dissociation, generated the alkene complex **B**. Density functional theory studies supported the preferential coordination of ketones, aldehydes, and alkenes

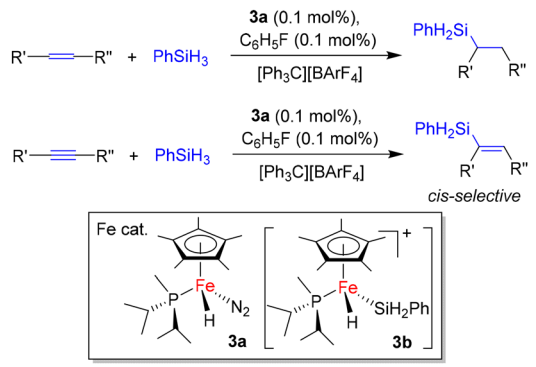

Scheme 5 An iron hydride complex **3**, used for the hydrosilylation of alkene and alkynes.

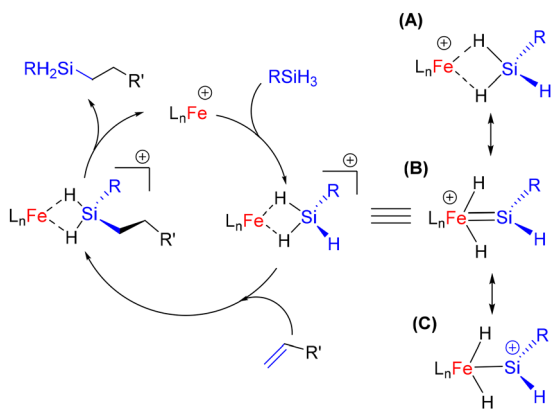

Fig. 7 Proposed mechanism *via* cationic Fe-silylene complex **3**.

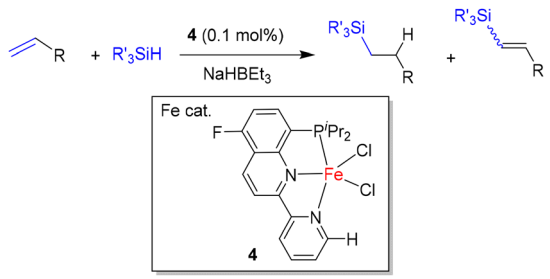

Scheme 6 The hydrosilylation of alkenes with PNN-type Fe pincer complex.

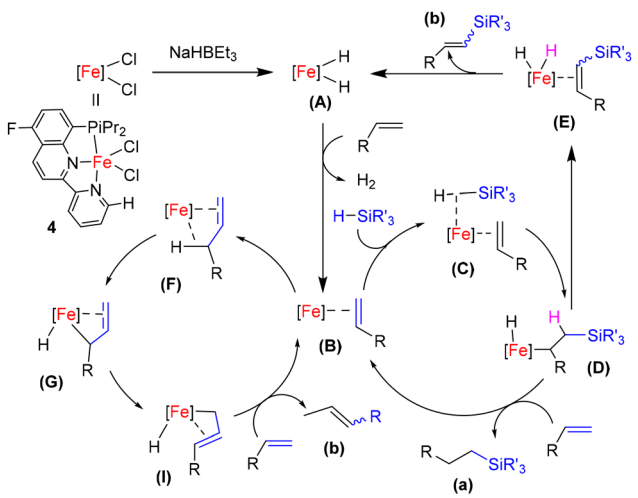

Fig. 8 Proposed mechanism using a PNN pincer-type complex for hydrosilylation of alkene.

over silanes at the Fe centre. Subsequent Si–H bond cleavage of the silane enabled silyl insertion into the coordinated alkene, converting **B** to **D**.[70] Completion of the catalytic cycle occurred *via* reductive elimination of the hydrosilylated product **a**, followed by alkene coordination to regenerate **B**. In contrast, β-hydride elimination from **D** to **E** leads to a dehydrogenative silylation pathway, forming a vinylsilane by-product, which further results in the formation of product **b**. Suppression of this β-hydride elimination pathway was therefore essential to favour formation of **a**. When they varied the substituents on phosphorus to Ph, iPr and Cy, the steric demand of the ligand, as quantified by %VBur within approximately 4.5 Å of the Fe centre, increased in the order Ph < iPr < Cy. Notably, increasing the $\%V_{Bur}$ enhanced product selectivity, indicating that bulkier ligands effectively inhibit β-hydride elimination.[68]

In 2021, Liu and Huang synthesised Fe complex **5** specifically for the regio- and stereoselective hydrosilylation of 1,3-enynes to access 1,3-dienylsilanes. The authors screened a range of tridentate ligands to optimise catalytic performance. Initial tests showed that Fe complexes bearing pyridinediimine, phosphine–bipyridine, and phosphinite–iminopyridine ligands provided high conversions but poor selectivity. A breakthrough was achieved with the use of an iminopyridine–oxazoline (IPO) ligand. Notably, replacing one oxazoline arm of a pyridinebisoxazoline ligand with an imine led to a marked improvement in both regioselectivity and yield. Complex **5**, featuring a sterically bulky *tert*-butyl group on the oxazoline ring and diphenylmethyl substituents at the *ortho* positions of the *N*-aryl group, significantly enhanced catalytic activity and regioselectivity, delivering the desired 1,3-dienylsilane with a product ratio exceeding 38 : 1 (Scheme 7). The tridentate IPO ligand effectively directed the *syn*-addition of the Si–H bond across the alkyne.[71]

In 2022, Banach and Pawluc reported a notable advancement in Fe-catalysed hydrosilylation of terminal aryl alkynes. Fe complex **6** bearing an NNN-tridentate hydrazone ligand was identified as an efficient catalyst for the formation of geminal bis(silanes). Among the ligand variants, complex **6a** exhibited exceptionally high catalytic efficiency in the Markovnikov-selective double hydrosilylation of terminal aryl alkynes (Scheme 8). Ligand modifications, such as replacing the NH group with NMe (**6b**) or altering the heterocycle orientation, resulted in significantly diminished or nearly suppressed catalytic activity,

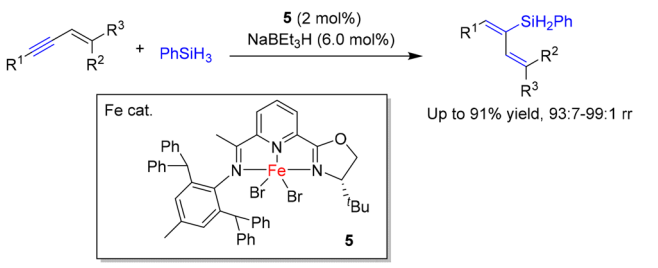

Scheme 7 The regio- and stereoselective hydrosilylation of 1,3-enyne.

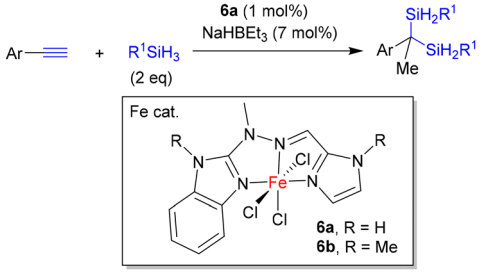

Scheme 8 The hydrosilylation of aryl alkynes by tridentate NNN Fe complex.

underscoring the critical role of both the NH functionality and the five-membered binding geometry. Furthermore, sodium triethylborohydride ($NaHBEt_3$) acts not only as a reductant for the Fe centre but also as a base, deprotonating the NH group to generate a ligand–BEt_3 adduct. The authors proposed that the formation of the N–BEt_3 bond from **6a** contributed to the significant improvement in catalytic activity compared to **6b**, which has NMe instead of NH in **6a**. NMR studies supported the formation of Fe–H intermediates upon catalyst activation, providing insight into the nature of the active species.[72]

In 2022, Zhu and co-workers employed a specially designed 2-imino-9-aryl-1,10-phenanthroline ligand for Fe-catalysed hydrosilylation of alkenes. This ligand played a decisive role in achieving high catalytic activity and exceptional regioselectivity in the hydrosilylation of alkenes and conjugated dienes. Fe complexes **7** bearing this ligand framework predominantly catalysed highly selective 1,2-anti-Markovnikov hydrosilylation of aryl-substituted and 1,1-dialkyl-substituted 1,3-dienes (Scheme 9). The sterically demanding ligand environment suppressed chelation of the diene to the metal centre and directed hydride transfer to the substituted carbon atom, thereby favouring formation of linear silane products. Moreover, variation of substituents on the *N*-aryl group significantly influenced both reaction rates and regioselectivity, further highlighting the steric control exerted by the ligand framework.[73]

Mechanistic investigations suggested that the reaction proceeds *via* a Chalk–Harrod-type Fe(0)/Fe(II) catalytic cycle, in which steric effects play a decisive role in controlling the

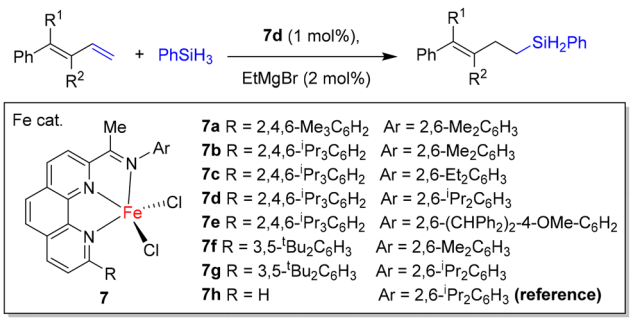

Scheme 9 Fe-catalysed hydrosilylation of conjugated dienes by 2-imino-1,10-phenanthrolines ligand.

observed 1,2-anti-Markovnikov selectivity. The Fe catalyst initially coordinates to both the olefin and the silane to form intermediate **A**. This species then undergoes ligand-to-ligand hydrogen transfer (LLHT) through a transition state (**TS-1**), generating an Fe(II) intermediate **B**. This hydrogen-transfer step is critical in determining the reaction's regioselectivity. Among the two possible transition states, **TS-1a** and **TS-1b**, **TS-1a** is favoured owing to reduced steric repulsion, whereas **TS-1b** suffers from significant steric interactions between the conjugated diene substrate and the bulky substituents of the 2-imino-9-aryl-1,10-phenanthroline ligand (Fig. 9). The sterically congested ligand environment surrounding the relatively small Fe centre enables precise discrimination between sterically distinct sites on the substrate, resulting in high regioselectivity governed by kinetic control. Following the formation of intermediate **B**, the catalytic cycle proceeds *via* reductive elimination through **TS-2**, affording the hydrosilylation product **C** and regenerating the active Fe catalyst **A**. Supporting evidence from deuterium-labelling experiments and kinetic isotope effect (KIE) studies indicates that the conversion of **A** to **B** is reversible, providing further validation of the proposed mechanistic pathway.[73]

Subsequent investigations by Zhu and co-workers in 2023 focused on the stereoconvergent 1,4-hydrosilylation of conjugated dienes using Fe complex **8** bearing α-diimine ligands. In particular, complexes incorporating bulky *N*-aryl substituents, such as *N*-2,6-diisopropylphenyl groups, generated an extremely congested environment around the Fe centre, thereby enforcing *cis*-coordination of *E*/*Z* diene mixtures (Scheme 10). This trend was evident from comparisons across a series of *N*-aryl ligands, in which increasing steric hindrance consistently led to enhanced regio- and stereoselectivity. In addition, the ligand backbone exerted a measurable influence on catalytic performance; for example, the cycloheptane-based complex **8b** resulted in diminished yields and reduced selectivity.[74]

Mechanistic studies of the Fe-catalysed stereoconvergent 1,4-hydrosilylation revealed a distinctive two-electron redox pathway, rather than radical or classical metal–hydride mechanisms commonly observed in related transformations. A defining feature of the α-diimine ligands is their ability to create a sterically congested environment around the Fe centre, which enforces *cis*-coordination of the conjugated diene irrespective of its *E*/*Z* configuration to form a cisoid intermediate **A**. This enforced coordination is crucial, as it enables ligand-to-ligand hydrogen transfer (LLHT) and subsequent formation of a π-allyl Fe intermediate. The use of a non-protic solvent was also essential to maintain *cis*-coordination and to promote the formation of the anti-π-allyl Fe intermediate. This pathway is kinetically favoured and leads exclusively to *Z*-allylsilane products. Although two π-allyl isomers, ***anti*-B** and ***syn*-B′**, are in principle accessible, only ***anti*-B** proceeds efficiently, as formation of ***syn*-B′** is unfavoured due to severe steric repulsion. The equilibrium between these intermediates is dynamic and reversible, ultimately resulting in the selective accumulation of the kinetically favoured ***anti*-B** species. Intermediate ***anti*-B** subsequently undergoes a π–σ rearrangement to generate intermediate **C**, which contains a *Z*-configured olefin. Reductive elimination from **C** then delivers the hydrosilylation product and regenerates intermediate **A** (Fig. 10). Furthermore, reactions conducted using a preformed Fe(0) complex reproduced the high yield and selectivity observed under catalytic conditions without the need for external reductants, indicating that a formal Fe(0)/Fe(II) redox cycle operates in this transformation.[74]

A significant advance in Fe-catalysed (*E*)-selective hydrosilylation of internal alkynes was reported by Chikkali and coworkers in 2024. The authors employed a low-valent Fe(0) complex **9**, [Fe(CO)$_3$(BDA)] (BDA = benzylideneacetone), in combination with a series of phosphine ligands (**L1–L5**) and systematically evaluated the catalytic performance (Scheme 11). The nature of the phosphine ligand exerted a pronounced influence on both conversion and stereoselectivity;

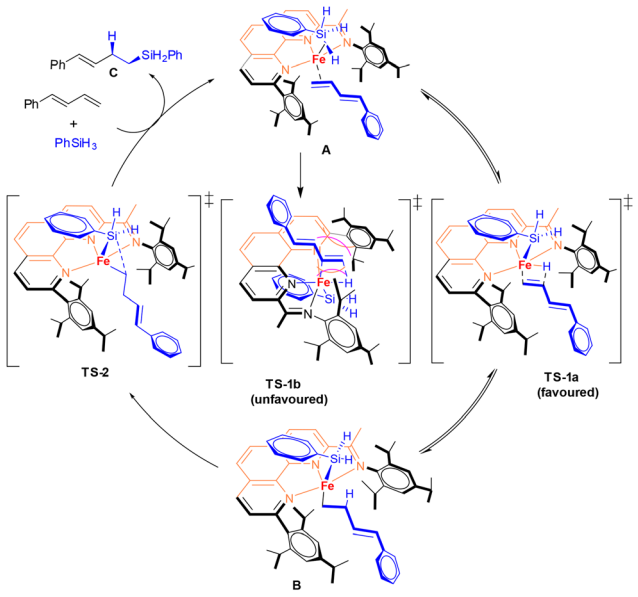

Fig. 9 Plausible mechanism for the regioselective system using complex **7d**.

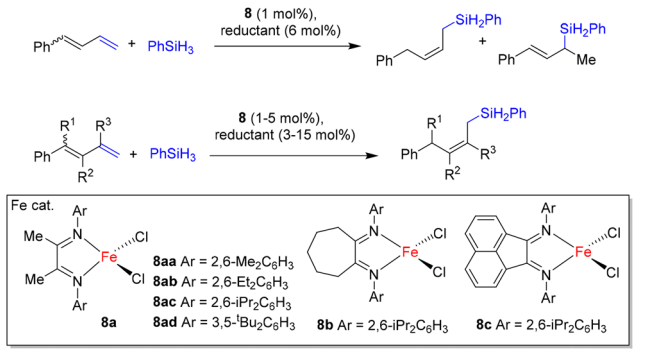

Scheme 10 Stereoconvergent 1,4-hydrosilylation of conjugated dienes catalysed by complexes **8**.

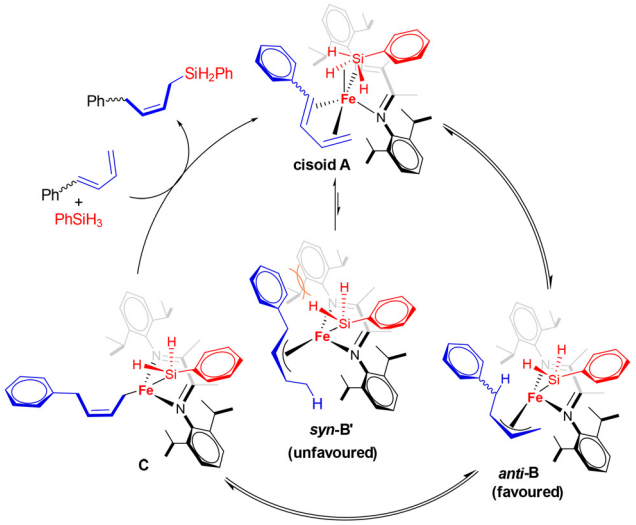

Fig. 10 A plausible catalytic cycle for stereo- and regioselective hydrosilylation.

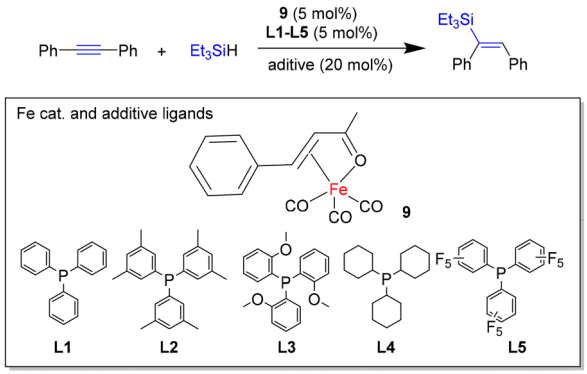

Scheme 11 Hydrosilylation of internal alkyne catalysed by a Fe $(CO)_3$(benzylideneacetone)/$P(C_6F_5)_3$ system.

notably, $P(C_6F_5)_3$ (**L5**) delivered the highest activity and (*E*)-selectivity. Interestingly, increasing the phosphine loading beyond an optimal level led to diminished catalytic activity, highlighting a delicate balance between ligand coordination at the Fe centre and effective substrate activation. Importantly, the hydrosilylation proceeded efficiently without the need for external activators or additives, underscoring the intrinsic reactivity of the Fe(0) catalytic system.[75]

Mechanistic investigations provided comprehensive insight into the Fe-catalysed (*E*)-selective hydrosilylation of internal alkynes, establishing a two-electron pathway operating through a formal Fe(0)/Fe(II) redox cycle. Density functional theory (DFT) calculations were employed to elucidate the catalytic process. Initial coordination of ligand **L5** to the Fe(0) complex **9** generated intermediate **Int-1** in an endergonic step. Subsequent oxidative addition of $HSiEt_3$ to the Fe centre formed the exergonic Fe(II) silyl–hydride intermediate **Int-2**. Dissociation of **L5** from **Int-2** led to intermediate **Int-3**, featuring an agostic interaction involving the γ-hydrogen, followed by coordination of the alkyne substrate to afford intermediate **Int-4** *via* a relatively endergonic process. All phosphine ligands (**L1–L5**) were evaluated computationally to assess ligand effects on reactivity, revealing that dissociation of **L5** from **Int-2** was significantly more favourable than that for ligands **L1–L4**, consistent with the experimentally observed superior performance of **L5**. From **Int-4**, two competing pathways were identified: migratory insertion of the alkyne into the Fe–H bond (classical Chalk–Harrod pathway) or into the Fe–Si bond (modified Chalk–Harrod pathway). DFT calculations indicated that the classical Chalk–Harrod pathway led to intermediate **Int-4a**, which was thermodynamically more favourable than the corresponding intermediate **Int-4b** formed *via* the modified pathway. Subsequent reductive elimination afforded the (*E*)-hydrosilylation product and regenerated a low-valent $Fe(CO)_3P(C_6F_5)_3$ species (Fig. 11). Finally, coordination of BDA to Fe $(CO)_3P(C_6F_5)_3$ completed the catalytic cycle.[75]

The earliest example of efficient Fe-catalysed, magnesium cation–supported hydrosilylation of alkynes using bathocuproine (bcp), a commercially available non-innocent bidentate ligand, was reported by Lefèvre and co-workers in 2024. Bathocuproine exhibits a distinctive dual role: it stabilises the Fe centre in a low-valent state and simultaneously promotes catalytic activity through participation in electron delocalisation. The complex $Fe(bcp)_2$ (**10b**), featuring two bcp ligands coordinated to Fe, was generated *in situ* by reaction of the precursor $FeCl_2$(bcp) (**10a**) with EtMgBr and additional bcp (Scheme 12). The robust coordination environment of **10b** rendered the complex resistant to decomposition, conferring

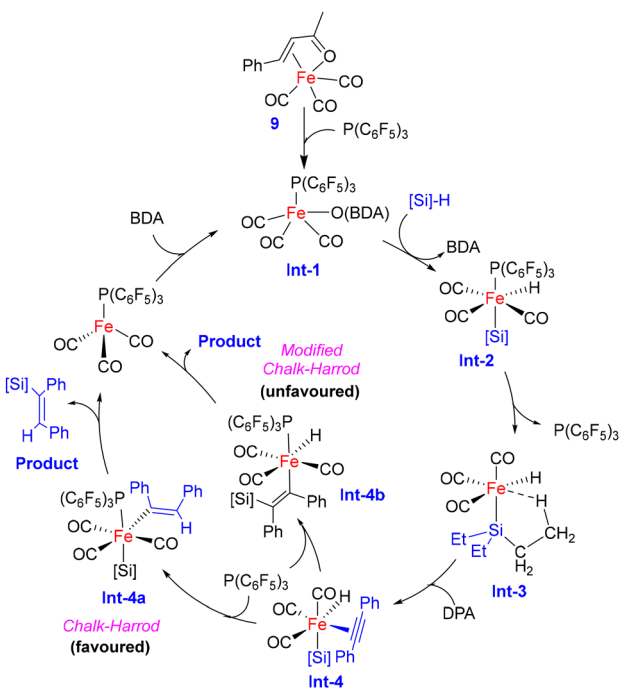

Fig. 11 A plausible mechanism for the hydrosilylation of alkyne using complex **9**.

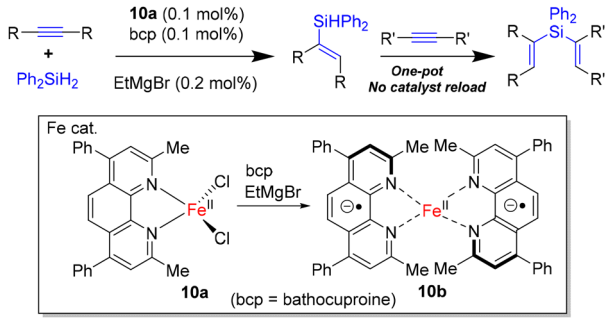

Scheme 12 Fe-catalysed hydrosilylation of alkyne facilitated by Fe $(bcp)_2$ (bcp = bathocuproine).

stability even under harsh thermal conditions. Notably, no loss of catalytic activity was observed after completion of the reaction, and upon addition of further alkyne substrate and exposure to more demanding conditions, a second hydrosilylation cycle also proceeded efficiently.[76]

Mechanistic studies of the hydrosilylation mediated by complex **10** were conducted to elucidate the catalytic pathway. The catalyst precursor **10a** is reduced by EtMgBr to generate **10b**, concomitantly producing a Lewis-acidic Mg^{2+} cation. This Mg^{2+} species plays a decisive role by abstracting one bcp ligand from the otherwise stable resting state **10b**, thereby generating the catalytically active monoligated Fe(bcp) species. Infrared spectroscopy supported the formation of an alkyne-bound intermediate **I**, arising from coordination of the alkyne to Fe(bcp). Subsequent activation of the Si–H bond occurs *via* oxidative hydrometallation through transition state **II**, leading to the formation of an alkenyl–Fe(III) intermediate.[59,77] The origin of the high α-selectivity was attributed to the chelating nature of the bcp ligand: coordination of this ligand at the Fe centre in **I** directs hydride transfer to the β-position opposite the chelating group. This process results in the formation of the α-Fe intermediate **III**, which undergoes reductive elimination to furnish the α-vinylsilane product and regenerate Fe (bcp) species (Fig. 12). Consistent with the observed *syn*-selectivity, the Fe-vinyl intermediate **III** does not undergo *Z*/*E* isomerisation on the catalytic time scale *via* a carbene-type pathway.[78,79] This reversible speciation is enabled by the non-innocent nature of the bcp ligand in conjunction with the Lewis-acidic Mg^{2+} cation, effectively circumventing the typical trade-off between catalyst stability and activity that often limits low-valent Fe catalysis.[76]

Recently, Punji and co-workers (2025) described a phosphine-free Fe(II)-catalysed protocol for the hydrosilylation of alkynes under mild conditions. A series of well-defined (NNN)-ligated Fe(II) complex dimers, **11a–11d**, were synthesised and evaluated for the efficient hydrosilylation of terminal and internal alkynes. At room temperature, *syn*-selective vinylsilanes were obtained with excellent regio- and stereoselectivity using only 1.5 mol% catalyst loading (Scheme 13). The reaction predominantly afforded monohydrosilylated products, thereby suppressing oligomerisation and over-reduction. The

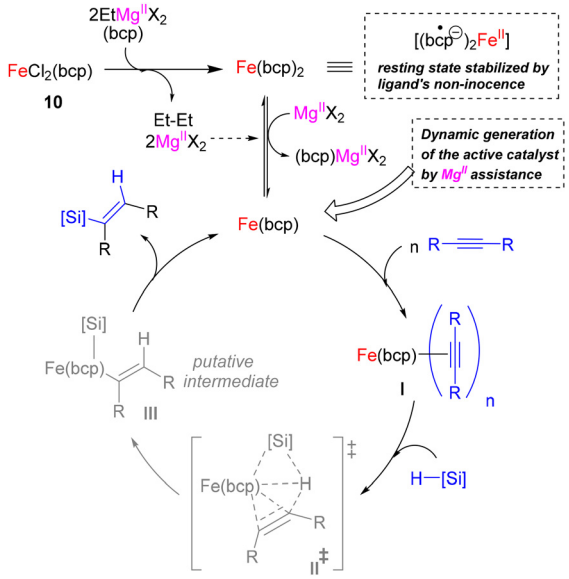

Fig. 12 Proposed mechanism for $Fe(bcp)_2$-mediated alkyne hydrosilylation, which included the generation of active species in response to Lewis-acidic Mg^{2+} cation.

catalytic system demonstrated broad substrate scope and good functional group tolerance, highlighting its synthetic utility.[80]

The mechanistic proposal for this system is primarily based on experimental investigations[80] and complemented by DFT calculations (Fig. 13).[81,82] The phosphine-free (NNN)-ligated Fe (II) complex **11** was found to operate *via* a redox-neutral catalytic pathway. In the presence of NaO^tBu, the binuclear Br-bridged precatalyst generates a mononuclear Fe(II) species **C** bearing a coordinated alkoxide ligand. Upon reaction with Ph_2SiH_2, complex **C** forms an Fe-silyl species **D**. The absence of detectable Ph_2HSiO^tBu by GC and MALDI analyses and control experiments involving reaction with triphenylcarbenium salts and phenylacetylene supported the conclusion that the classical pathway *via* Fe–H formation is unlikely.

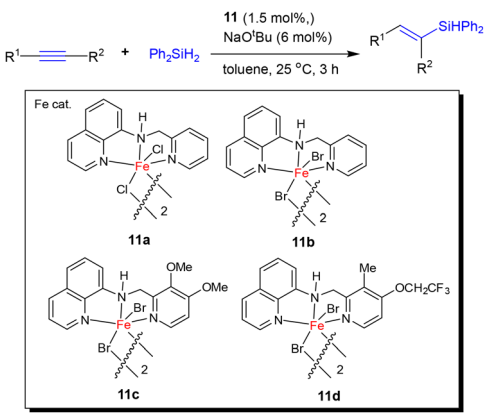

Scheme 13 A phosphine-free (NNN)Fe(II) catalysed *syn*-selective hydrosilylation of alkynes with diphenyl silane by using complexes **11a–11d**.

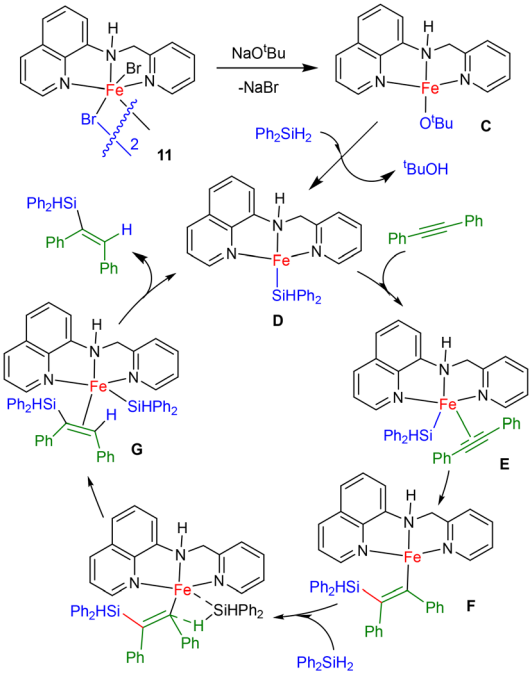

Fig. 13 Plausible mechanistic cycle for hydrosilylation of alkyne by using complex **11b**.

Coordination of diphenylacetylene to complex **D** affords the η^2-bound intermediate **E**, which undergoes migratory insertion of the silyl group to generate Fe-vinyl species **F**. Subsequent reaction with silane delivers intermediate **G** and releases the *syn*-configured vinylsilane product, regenerating active species **D**. DFT calculations support this redox-neutral silyl-migration pathway and rationalise the observed regio- and stereoselectivity, favouring *syn*-addition and formation of thermodynamically stable β-(*E*) vinylsilane products.[80]

Recently, Wang and Zhao's group (in 2025) reported a highly selective construction of silicon-stereogenic benzosilacycles *via* an Fe-catalysed sequential hydrosilylation strategy using complexes **12a–12f** (Scheme 14). This procedure enables regio-, diastereo-, and enantioselective hydrosilylation of *o*-alkenylphenyl silanes with alkynes, affording 5-, 6-, and 7-membered benzosilacycles in good to excellent yields. Curiously, high stereoselectivity was achieved, with regioselectivities up to 95 : 5, diastereoselectivities up to 95 : 5, and enantioselectivities reaching 99% ee. The protocol further allows triple hydrosilylation, providing access to chiral benzosilacycles bearing fully carbon-substituted silicon stereocentres.[83]

They suggested a mechanism in which the Fe catalyst promotes sequential hydrosilylation through a controlled and stepwise activation of Si–H bonds (Fig. 14). The catalytically active Fe-silyl species **A** is generated upon reduction of the Fe (II) precatalyst by $NaBHEt_3$ in the presence of silane **F**.[50,84,85] The authors did not determine the oxidation state of the Fe intermediates, but proposed a redox-neutral catalytic pathway. Insertion of the alkene into the Fe–Si bond of species **A** affords

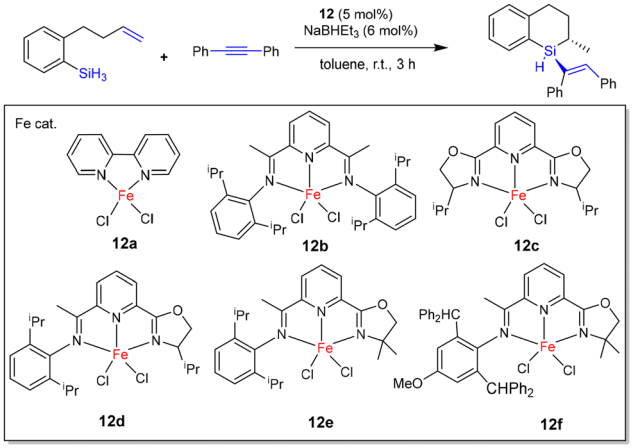

Scheme 14 Iron-catalysed sequential hydrosilylation of alkynes with 2-vinylphenyl silanes by using complex **12a–12f**.

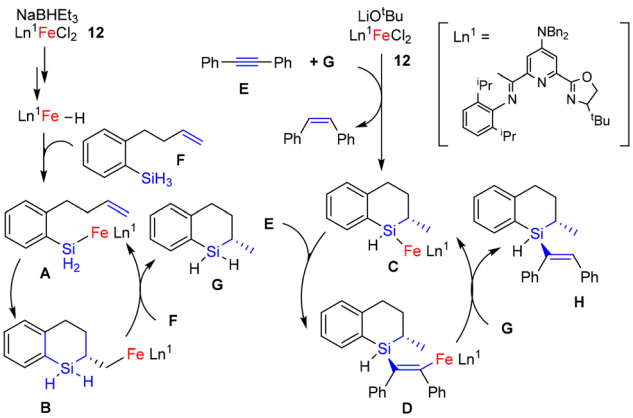

Fig. 14 Proposed mechanism for sequential hydrosilylation of alkyne started from intramolecular hydrosilylation and followed by intermolecular hydrosilylation by using complex **12**.

the corresponding Fe-alkyl intermediate **B**, which subsequently undergoes σ-bond metathesis with silane **F** to regenerate Fe-silyl species **A** and release the hydrosilylation product **G**. Further reaction of **G** with complex **12** furnishes Fe-silyl intermediate **C**. Kinetic studies suggest that the active Fe-silyl intermediate **C** exists in equilibrium with its dimeric form. Subsequent insertion of alkyne **E** into the Fe–Si bond of **C** generates Fe–alkenyl intermediate **D**, which reacts with **G** to regenerate Fe-silyl species **C** and deliver the final product **H**. Overall, the transformation proceeds through migratory insertion and σ-bond metathesis steps, and no change in the iron oxidation state was established in the original report.

2.2 Hydrosilylation of carbonyl compounds

An unresolved mechanistic case of Fe-catalysed hydrosilylation of carbonyl compounds was reported by Findlater and coworkers in 2019. The authors investigated Fe(0)-catalysed hydrosilylation of aldehydes using the well-defined complex Fe(BIAN)(η^6-toluene) (**13**), where BIAN denotes 1,2-((bis-2,6-diiso-

propylphenyl)imino)acenaphthene. The BIAN ligand provides substantial steric shielding together with strong π-accepting properties, thereby modulating the electronic environment of the Fe centre and enhancing catalytic performance. The reaction proceeded efficiently without additives, selectively converting aldehydes and ketones into silyl ethers, which upon hydrolysis yielded the corresponding alcohols (Scheme 15). Aromatic aldehydes, heteroaromatic aldehydes (*e.g.*, pyridine- and thiophene-based substrates) and aliphatic aldehydes, including linear and branched substrates, were successfully converted.[86]

Two plausible reaction mechanisms were evaluated using density functional theory (DFT) calculations in conjunction with experimental observations. Depending on the mode of silane approach to the metal centre, two distinct reaction pathways (**A** and **B**) can operate *via* the same prochiral Fe intermediate, **A1**/**B1**, generated by ligand exchange of η^6-toluene with benzaldehyde. Pathway **A**, which was energetically favoured, proceeds through two key elementary steps: initial hydride transfer from coordinated diphenylsilane (Ph_2SiH_2) to benzaldehyde (PhCHO), followed by Si–O bond formation *via* transition states **ATS1** and **ATS2**, respectively (Fig. 15). In contrast, the less favourable pathway **B** involves a σ-bond metathesis between the Si–H bond and the Fe–O bond in intermediate **A3**. Importantly, the theoretical analysis revealed that the reaction proceeds through a spin-crossover process, commonly referred to as a two-state reactivity (**TSR**). Along the reaction coordinate, the Fe(0) centre can access multiple spin states, namely singlet (S = 0), triplet (S = 1), and quintet (S = 2), which contribute to the overall reaction pathway.

In 2020, Li and co-workers synthesised a new pincer-type [PSiP] Fe complex **14** for the hydrosilylation of carbonyl compounds. The ligand was deliberately designed to incorporate two phosphine arms (–PPh_2 or –$PiPr_2$) flanking a central silyl donor, thereby creating a rigid and electron-rich coordination environment around the Fe centre. Among five different [PSiP]-pincer Fe(II) hydride complexes evaluated, complex **14** bearing bulky isopropyl substituents on the phosphorus atoms exhibited the highest catalytic activity (Scheme 16). Notably, the addition of pyridine *N*-oxide (typically 5 mol%) was found to significantly enhance reaction efficiency. Control experiments indicated that, in the absence of the *N*-oxide additive, the reaction proceeded sluggishly, demonstrating that the additive plays a crucial role. This ligand system displayed broad functional-group tolerance and afforded excellent yields under mild conditions.[87]

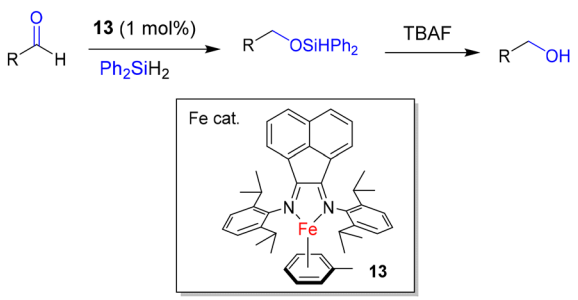

Scheme 15 Hydrosilylation of aliphatic and aromatic aldehydes using complex **13** as a catalyst.

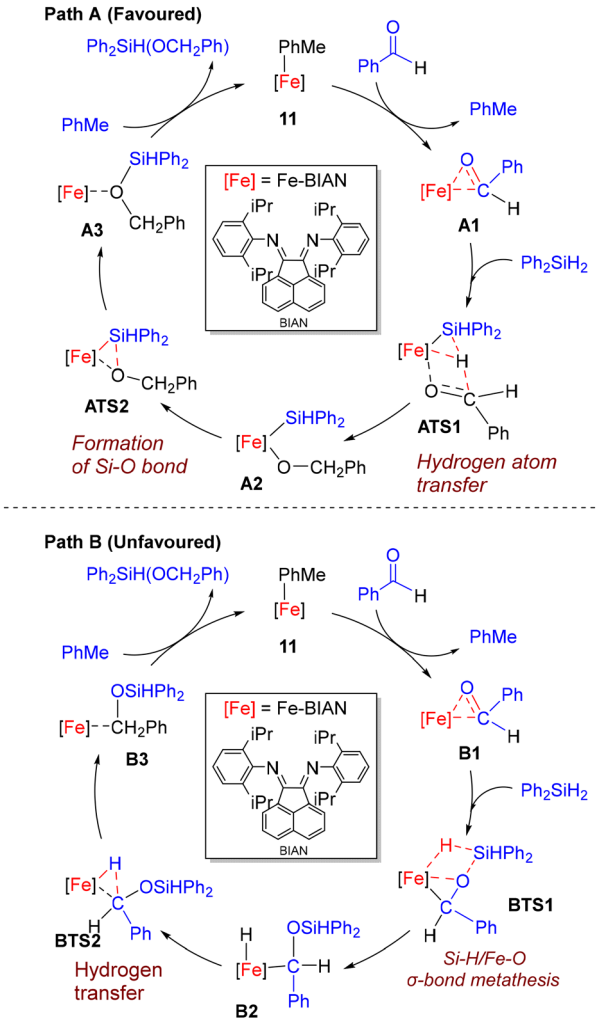

Fig. 15 Proposed reaction pathways for hydrogen transfer: Path A involves Si–O bond formation, whereas Path B proceeds *via* σ-bond metathesis of the Si–H/Fe–O bond.

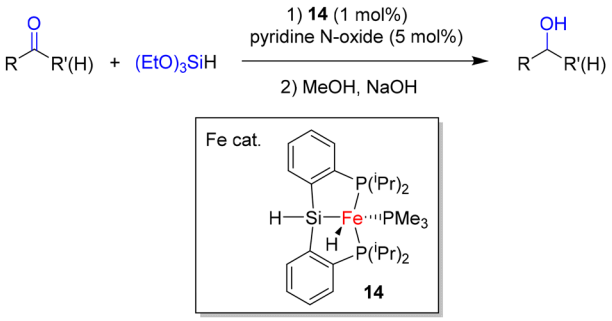

Scheme 16 Complex **14** with a strong σ-donor ligand accelerated the hydrosilylation of carbonyl compounds in the presence of pyridine *N*-oxide.

The catalytic mechanism was proposed for the hydrosilylation of carbonyl compounds using complex **14** as the pre-catalyst. Pyridine *N*-oxide facilitates the dissociation of one PMe_3 ligand from the Fe centre by forming stable $O{=}PMe_3$, thus generating the unsaturated active Fe–H species **A**. Coordination of the carbonyl substrate to **A** affords intermediate **B**, followed by migratory insertion of the carbonyl group into the Fe–H bond to yield alkoxide intermediate **C**. Subsequent reaction of **C** with $(EtO)_3SiH$ proceeds *via* a four-membered [Fe–O–Si–H] σ-bond metathesis transition state **D**, delivering the corresponding silyl ether product and regenerating the active species **A** (Fig. 16). This mechanistic proposal is supported by *in situ* NMR and IR studies. A signal at δ 31.8 ppm in the ^{31}P NMR spectrum was assigned to liberated $OPMe_3$, confirming PMe_3 dissociation upon addition of pyridine *N*-oxide. Moreover, a new resonance at δ −10.16 ppm in the ^{1}H NMR spectrum, together with an Fe–H stretching vibration at 1937 cm^{-1} observed by IR spectroscopy, provided direct evidence for the formation of the Fe–H intermediate **A**. The presence of bulky and electron-donating isopropyl substituents on the phosphine arms of the [PSiP] ligand facilitates PMe_3 dissociation and promotes the insertion–metathesis sequence by stabilising the reactive intermediates involved in the catalytic cycle.[87]

Well-defined NHC–Fe complexes were also investigated by Albrecht and co-workers in 2021, who reported a series of Fe complexes **15** for the hydrosilylation of aldehydes. These catalysts were based on a modular piano-stool architecture incorporating cyclopentadienyl (Cp) or pentamethylcyclopentadienyl (Cp*) ligands in combination with NHC donors. The NHC ligands were systematically varied across two main classes, imidazolylidenes and triazolylidenes, with different wing-tip substituents (methyl, isopropyl, isobutyl, and mesityl) introduced to probe steric and electronic effects. In general, incorporation of the bulkier Cp* ligand generally diminished catalytic activity due to increased steric congestion at the metal centre, although it proved beneficial for reactions involving sterically demanding substrates (Scheme 17).[88]

In 2021, Sun and co-workers developed a novel N-heterocyclic silylene (NHSi) ligand incorporated into Fe complex **16**, which enabled the hydrosilylation of both aldehydes and ketones under identical mild conditions. The corresponding Fe(II) hydride complex, $[Si,C]FeH(PMe_3)_3$ (**16**), was synthesised *via* $C(sp^3)$–H bond activation of the NHSi ligand precursor using $Fe(PMe_3)_4$. The NHSi ligand forms a robust five-membered chelate through coordination of the silylene silicon atom and a carbon atom derived from the *tert*-butyl group. In addition, the NHSi framework contributes to the observed chemoselectivity of the catalyst. The catalytic system operated efficiently under a nitrogen atmosphere without the need for additives. Under the optimised conditions, a broad range of aldehydes and ketones were smoothly reduced, affording the corresponding alcohols in yields of up to 99%, highlighting its excellent catalytic activity and broad substrate scope (Scheme 18).[89]

The mechanistic investigation centred on stoichiometric reactions of $[Si,C]FeH(PMe_3)_3$ (**16**) with either $(EtO)_3SiH$ or acetophenone as a representative carbonyl substrate, in order to probe the formation of key intermediates. Based on the experimental observations, together with insights from related literature, a plausible catalytic cycle was proposed involving

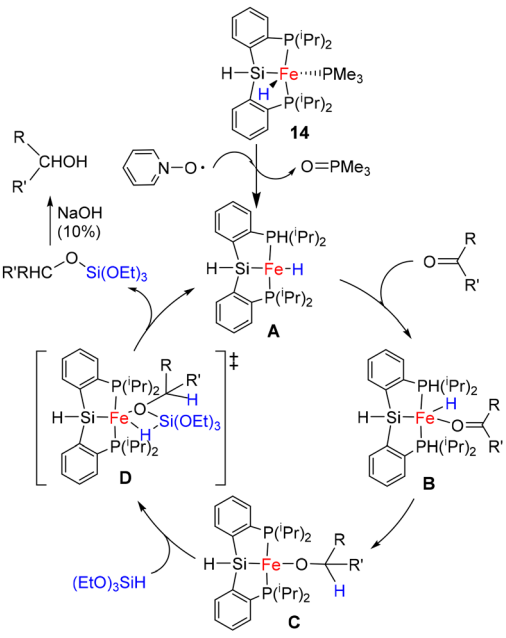

Fig. 16 Proposed mechanism for hydrosilylation of carbonyl compounds by the pincer-type [PSiP] Fe complex **14**.

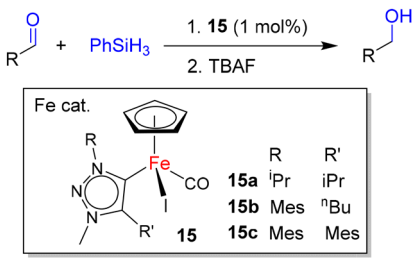

Scheme 17 Hydrosilylation of carbonyl compounds by piano-stool Fe complex **15**.

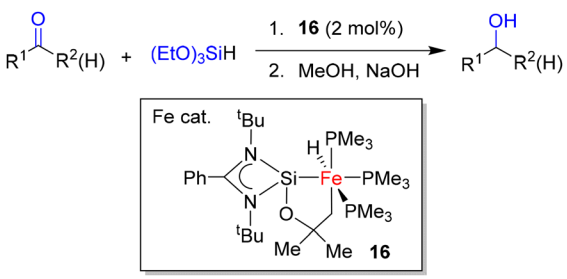

Scheme 18 Hydrosilylation of carbonyl compounds by using iron hydride complex **16**.

three principal steps. Initially, ligand exchange between complex **16** and the carbonyl substrate affords intermediate **A**. Subsequent migratory insertion of the carbonyl C═O bond into the Fe–H bond yields a metal alkoxide species (intermediate **B**). In the final step, σ-bond metathesis between the Fe-bound alkoxide and the silane produces the hydrosilylation product (silyl ether) and regenerates the active hydride complex **16**. Notably, both theoretical considerations and prior reports indicate that insertion of the carbonyl group into the Fe–H bond is energetically more favourable than insertion into a putative Fe–Si bond, which further supports the proposed mechanism (Fig. 17).

Xu, Cui, and co-workers reported in 2021 an anionic Fe complex **17**, $[CpFe(CO)_2]^-[M]^+$ (**17a**: M = K; **17b**: M = NEt_4), which exhibited remarkably high catalytic efficiency in the hydrosilylation of a broad range of aldehydes and ketones. This catalyst system is readily accessible, air-stable, and easy to handle. The structurally simple nature of complex **17** imparts a strong nucleophilic character to the Fe centre, enabling exceptionally high turnover frequencies (TOFs) of up to 24 540 h^{-1} under mild, solvent-free conditions using only 0.05 mol% catalyst loading with $PhSiH_3$ as the hydrosilane (Scheme 19). Moreover, the ligand system demonstrated excellent functional group tolerance and selectivity, particularly favouring aldehydes over ketones in competitive reactions. Its catalytic behaviour was attributed to the potential formation of reactive iron-hydride intermediates *via* oxidative addition of hydrosilane, although the exact mechanism remains under investigation.[90]

The longstanding question of whether Fe(II)–H or Fe(II)–Si species constitute the catalytically active intermediates in Fe-catalysed hydrosilylation was systematically investigated by Tonzetich and co-workers in 2022. To stabilise reactive Fe species, the authors employed a pyrrole-based pincer ligand, ^{cy}PNP, derived from 2,5-bis(dicyclohexylphosphinomethyl) pyrrole. This robust tridentate ligand framework enabled the isolation and characterisation of key catalytic intermediates, including an Fe hydride and an Fe silyl complex, namely [FeH$(N_2)(PMe_2Ph)(^{cy}$PNP)] (**18a**) and [Fe$(SiHPh_2)(^{cy}$PNP)] (**18b**), respectively (Scheme 20). Isolation of these complexes suggests that both the hydride and silyl pathways accessible, depending on the reaction conditions and substrates.[91]

Based on stoichiometric and kinetic studies, the proposed mechanism for carbonyl hydrosilylation involves two distinct pathways depending on the precatalysts (**18a** or **18b**) and the substrate. For aldehyde hydrosilylation with hydride complex **18a**, the carbonyl group readily inserts into the Fe–H bond to form an Fe–alkoxide intermediate. Subsequent σ-bond metathesis with hydrosilane regenerates the Fe–H species and releases the silyl ether product, consistent with the classical Chalk–Harrod mechanism. In contrast, the silyl complex **18b** does not operate through an analogous insertion pathway. Although aldehyde insertion into the Fe–Si bond to give a β-siloxyalkyl intermediate was observed, this species proved kinetically inert. Instead, experimental evidence supports an outer-sphere mechanism in which **18b** primarily activates the hydrosilane rather than undergoing direct insertion into a metal–ligand bond (Fig. 18). For ketone hydrosilylation, both **18a** and **18b** follow the outer-sphere mechanism, as steric effects disfavour direct ketone insertion into the Fe–H bond. Under these conditions, reaction of the hydride complex **18a** with hydrosilane generates the silyl species **18b** through σ-bond metathesis between the Fe–H and Si–H bonds, with concomitant release of H_2 *in situ*. The interconversion between hydride and silyl species *via* H_2 evolution enables dynamic catalyst speciation and sustained catalytic turnover, particu-

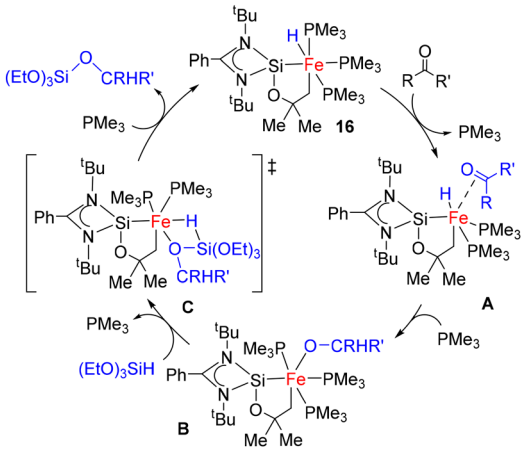

Fig. 17 A proposed mechanism of NHSi–Fe–H^- for hydrosilylation of carbonyl compounds.

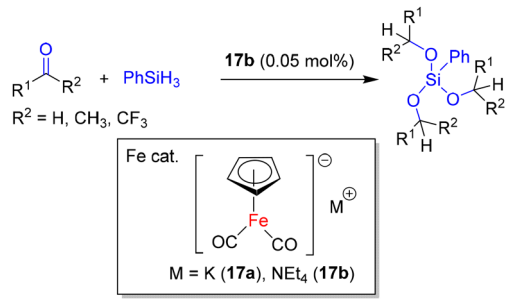

Scheme 19 Hydrosilylation of aldehydes and ketones using anionic Fe complex **17**.

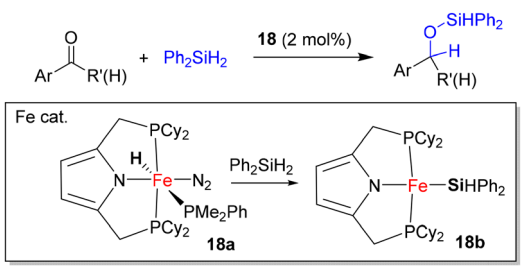

Scheme 20 Hydrosilylation of aromatic carbonyl compounds by PNP pincer-type Fe complexes **18**.

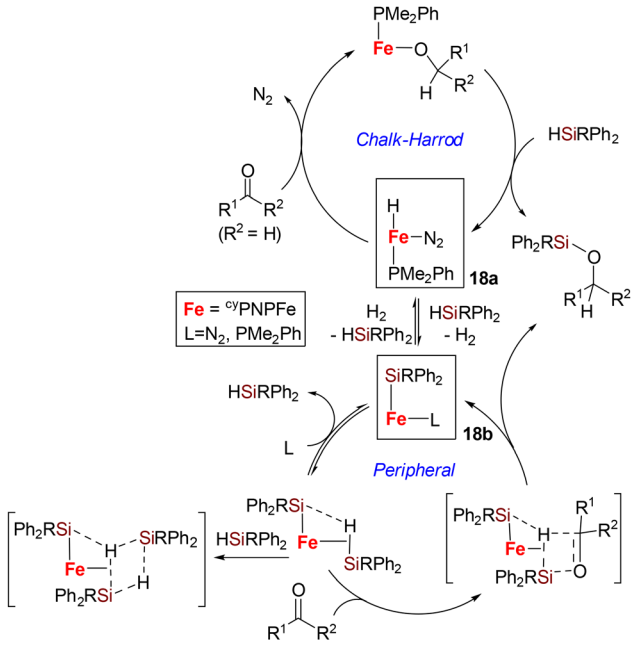

Fig. 18 A proposed mechanism for ^{cy}PNP–Fe catalysed hydrosilylation of carbonyl compounds.

larly for substrates that are otherwise unreactive toward **18b** alone.[91]

Matsubara and co-workers reported in 2023 that an Fe(II) catalyst, [Fe(MIC)(CO)$_2$Br][BPh$_4$] (**19**), efficiently promotes the hydrosilylation of aromatic aldehydes and ketones. The catalyst features a pincer-type ligand comprising two 1,2,3-triazolylidene meso-ionic carbene (MIC) units bridged by a pyridylene core, which creates a highly electron-rich coordination environment around the Fe centre. In addition, the bulky 2,6-diisopropylphenyl substituents on the MIC ligands play a key role in controlling substrate approach and selectivity (Scheme 21). Upon addition of KO^{t}Bu at room temperature, rapid CO evolution was observed. Density functional theory (DFT) studies revealed that the base is essential for activation of the Fe–Br precursor **19**, promoting a transmetallation process with HSi(OEt)$_3$ to generate an active Fe–H species, along with the formation of a silyl alkoxide, Si(O*t*Bu)(OEt)$_3$,

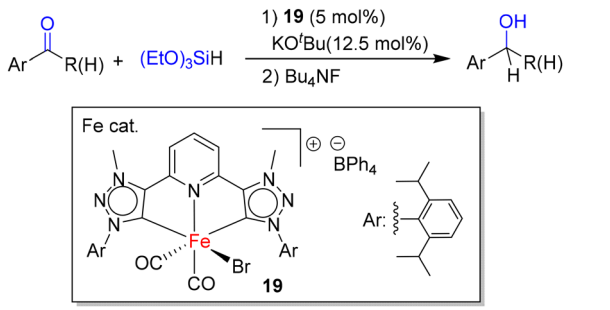

Scheme 21 The hydrosilylation of aromatic carbonyl compounds by MIC–Fe complex **19**.

and KBr. At this stage, following the exchange of hydrosilane and CO, the nucleophilic alkoxide ion on potassium coordinated to bromine attacks the silicon atom, forming Fe–H and K–Br bonds (Fig. 19). The $\Delta G_{298\ K}$ at the transition state (**TS$_{BC}$**) was estimated to be +23.0 kcal mol^{-1}. Notably, this activation mode demonstrates that generation of an active Fe-hydride from an Fe–halide precursor does not require a conventional hydride donor, highlighting an alternative base-assisted pathway for Fe–H formation in hydrosilylation catalysis.[92]

Well-defined PPyNP–Fe complexes **20** were reported in 2023 by Auffrant and co-workers as efficient catalysts for hydrosilylation reactions. These Fe-based systems are supported by a pincer-type PPyNP ligand incorporating phosphine, pyridine (lutidine), and iminophosphorane donor units. The ligand exhibits strong electron-donating ability due to the highly polarised P=N bond within the iminophosphorane fragment, enhancing both σ- and π-donation to the Fe centre. The Fe(II) complex [Fe(PPyNP)(OTf)$_2$] (**20a**) exists in solution as an equilibrium mixture of a solvent-free species and an acetonitrile-coordinated form, [Fe(PPyNP)(NCCH$_3$)$_3$]$^{2+}$ (**20b**), and these species are implicated in catalyst activation. Importantly, although coordination of *tert*-butyl isocyanide in place of acetonitrile in **20b** affords the dicationic tris(isocyanide) complex [Fe(PPyNP)(CN^{t}Bu)$_3$]$^{2+}$, this adduct does not generate the active catalyst under hydrosilylation conditions. Instead, treatment of the solvent-free/acetonitrile-bound precatalyst mixture with KHBEt$_3$ produces the catalytically active iron-hydride species *in situ*. Using 1 mol% catalyst loading, efficient hydrosilylation of acetophenone was achieved at room temperature (Scheme 22), affording near-quantitative conversion across a range of substituted derivatives.[93]

Sunada and co-workers in 2023 investigated Fe(II) complexes supported by σ-organosilyl ligands to enhance catalytic

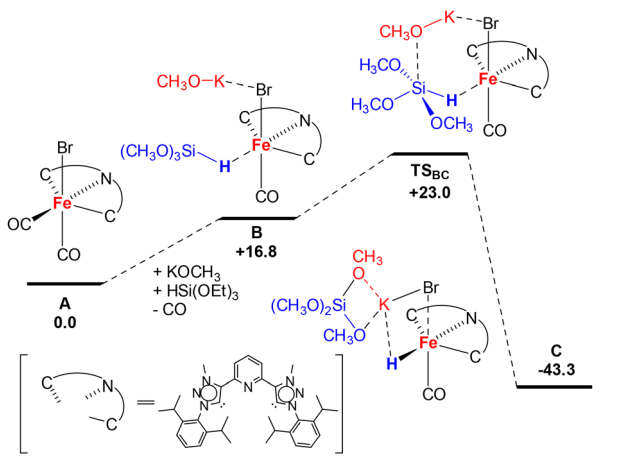

Fig. 19 Reaction path and the relative Gibbs free energies (kcal mol^{-1}) calculated by PCM(toluene)-B3LYP-D3BJ/6-311G(d,p)//B3LYP/ECP (Lanl2DZ) & 6-31G(d). Thermal energy corrections at the condition of 298.15 K and 1 atm were based on the harmonic vibrational analysis with B3LYP/ECP(Lanl2DZ) & 6-31G(d).

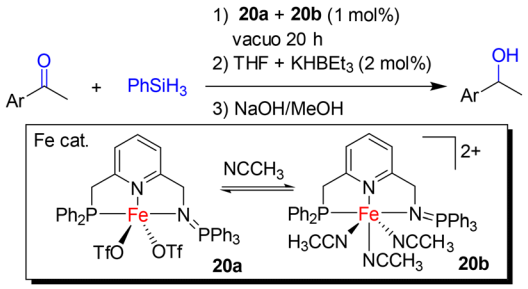

Scheme 22 PPyNP-supported Fe-catalysed hydrosilylation of acetophenone.

performance in the hydrosilylation of aromatic carbonyl compounds. Ligand exchange of the tetrahedral precursor complex $Fe(THF)_2[Si(SiMe_3)_3]_2$ (**21a**) with an N-heterocyclic carbene (NHC), such as 1,3-dimethyl-4,5-dimethylimidazol-2-ylidene (MeIMMe), afforded the square–planar complex *trans*-$(MeIMMe)_2Fe[Si(SiMe_3)_3]_2$ (**21b**). This complex exhibited markedly improved hydrosilylation activity (85% conversion) compared with the precursor **21a** (30%) in the reaction of acetophenone with TMDS (TMDS = 1,1,3,3-tetramethyldisiloxane). In particular, the σ-organosilyl ligand framework also enabled the formation of a *cis*-configured square-planar complex **21c**. Moreover, replacement of MeIMMe with a bulky cyclic (alkylamino)carbene (CAAC) led to the synthesis of a rare three-coordinate, planar Fe(II) bis(silyl) complex **21d**. Evaluation of these complexes in the hydrosilylation of acetophenone using Ph_2SiH_2 revealed that the square-planar *trans*-complex **21b** displayed the highest catalytic activity, achieving quantitative conversion (>99%) even at a low catalyst loading of 0.05 mol% (Scheme 23). The CAAC-supported three-coordinate complex **21d** also showed excellent performance (>99% conversion), whereas the *cis*-configured complex **21c** was slightly less active (85% conversion).[94]

This work was further extended by Sunada and co-workers in 2024 through the development of a monodentate σ-silyl ligand, $-Si(SiMe_3)_2(SiMe_2tBu)$, designed to generate planar three-coordinate Fe(II) complexes exhibiting enhanced catalytic activity in hydrosilylation reactions. This modified organosilyl ligand was derived from $-Si(SiMe_3)_3$ by replacing one $SiMe_3$ group with a bulkier $SiMe_2tBu$ substituent to increase steric demand. The increased steric congestion favoured the formation of coordinatively unsaturated species, leading to the exclusive synthesis of three-coordinate Fe(II) bis(silyl) complexes **22a** and **22b**. These complexes adopted an almost perfectly planar geometry and displayed shorter Fe–Si bond distances compared with previously reported four-coordinate analogues **21b** and **21c**. Structurally, complex **22a** contained a THF ligand, whereas complex **22b** was obtained *via* ligand exchange with the N-heterocyclic carbene MeIMMe (Scheme 24). Both complexes exhibited excellent catalytic performance with TMDS and Ph_2SiH_2, surpassing the activity of four-coordinate systems such as **21b**. Notably, complex **22a** achieved complete conversion within 20 minutes at room temperature using only 0.1 mol% catalyst loading.[95]

Wills and Khamis's group recently, in 2025, studied the synthesis and explored catalytic performance in hydrosilylation reactions of a series of well-defined Fe complexes (cyclopentadienone)Fe(NHC)$(CO)_2$ (**23a–23c**) bearing NHCs with strong σ-donor ability (Scheme 25). The resulting complexes were

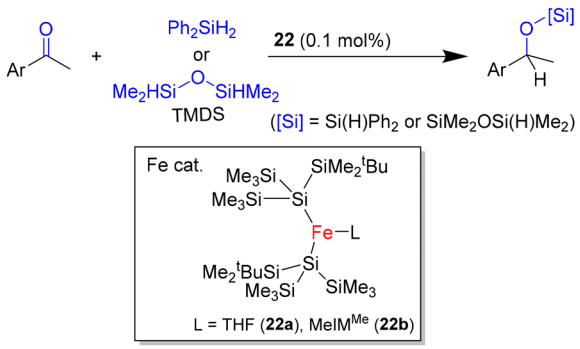

Scheme 24 Hydrosilylation of acetophenone by three-coordinate Fe(II) bis-silyl complex **22**.

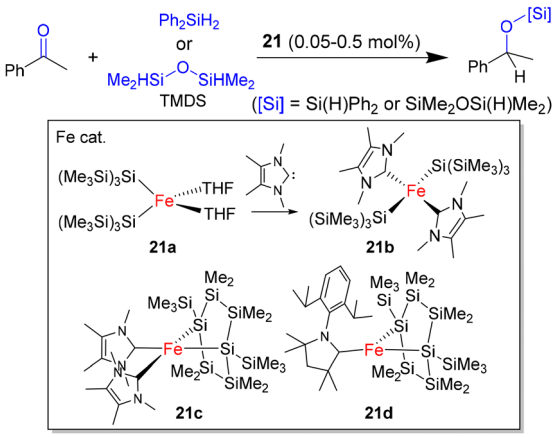

Scheme 23 Iron bis-silyl complexes for hydrosilylation of acetophenone.

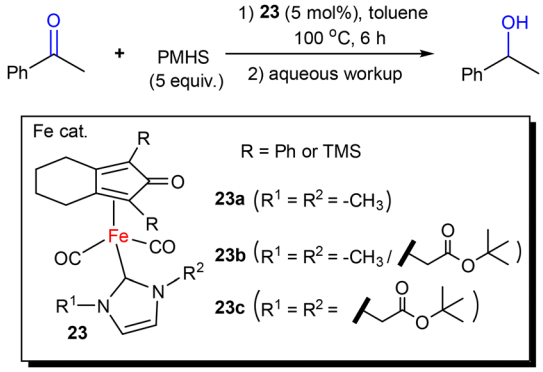

Scheme 25 Hydrosilylation of phenyl ketones with PMHS by using complex **23**.

readily accessible, air-stable, and displayed distinct reactivity profiles reliant on the NHC substituents. Approximately, some Fe–NHC systems exhibited good catalytic activity toward the hydrosilylation of unsaturated substrates under mild conditions. It was demonstrated that subtle ligand modifications in complexes **23a–23c** significantly influence catalytic outcomes, including activity and substrate tolerance.[96]

2.3 Hydrosilylation of carboxylic acids and derivatives

In early 2019, Findlater and co-workers reported an Fe-catalysed hydrosilylation of esters to the corresponding alcohols. Notably, optimal catalytic performance was achieved using 1 mol% of Fe complex **24** bearing a redox-active BIAN ligand in combination with 3 mol% *n*-BuLi as an activator. This catalyst, previously employed for aldehyde hydrosilylation (Scheme 15),[86] also demonstrated high efficiency toward ester reduction, including transformations using the cost-effective hydrosilane PMHS (Scheme 26). A broad range of substrates, including aliphatic, alicyclic, and electronically diverse esters bearing electron-donating or electron-withdrawing substituents, were converted in good to excellent yields. Mechanistic investigations suggested that treatment of complex **24** with three equivalents of *n*-BuLi generated an anionic Fe species *via* partial ligand dearomatisation, which served as the catalytically active form. Stepwise addition of *n*-BuLi resulted in distinct EPR signals, indicating the presence of multiple reactive intermediates or species (Fig. 20).[97]

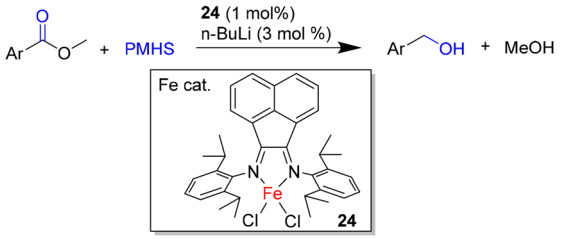

Scheme 26 Bidentate BIAN Fe(II) complex **24**, as active in hydrosilylation of esters.

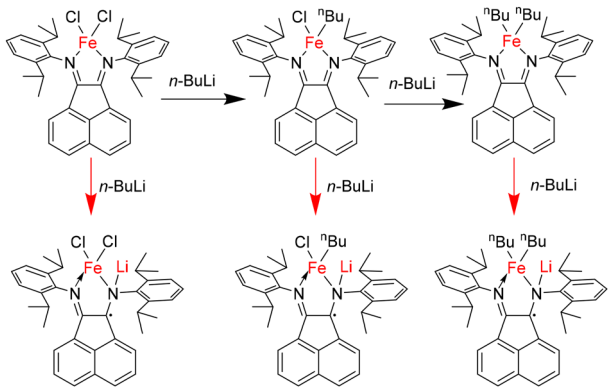

Fig. 20 Suggested reaction routes of complex **24** with *n*-BuLi. Red reaction arrows show complex reduction, whereas black response arrows show the processes of salt metathesis.

In 2019, Mandal and co-workers reported the catalytic reduction of nitriles to primary amines using a pentacoordinate Fe(III) complex **25** supported by a phenalenyl-derived ligand, H_2L [9,9′-(ethane-1,2-diylbis(azanediyl))bis(1*H*-phenalen-1-one)]. The redox-active ligand framework stabilizes the Fe centre and promotes catalytic activity in hydrosilylation reactions (Scheme 27). The catalytic system exhibited a broad substrate scope, efficiently converting aromatic, heteroaromatic, aliphatic, and sterically hindered nitriles into the corresponding primary amines by using PMHS as an inexpensive and environmentally benign hydride source. Aromatic nitriles bearing both electron-donating (–Me, –OMe) and electron-withdrawing (–F, –Cl, –Br, $–CF_3$) substituents afforded good to excellent yields. Sterically demanding substrates, such as 2,4,6-trimethylbenzonitrile, were also effectively reduced. Heteroaromatic nitriles, including 3-pyridinecarbonitrile, showed moderate conversion (≈55%), while various cyclic and acyclic aliphatic nitriles, as well as industrially relevant adiponitrile, were successfully transformed under the reported conditions.[98]

The earliest example of an efficient NHC–Fe(II)-catalysed hydrosilylation of CO_2 was reported by the Albrecht group in 2023. A series of piano-stool-type Fe(II) complexes bearing imidazolylidene and triazolylidene NHC ligands was evaluated for their catalytic activity in the conversion of CO_2 and amines into *N*-formamides, using phenylsilane ($PhSiH_3$) as the reducing agent. Among the complexes tested, the aryl-substituted triazolylidene complex **26** exhibited superior catalytic performance in THF under 1 bar CO_2 pressure with piperidine as the amine substrate (Scheme 28). Mechanistically, the reaction is proposed to proceed *via* initial silane activation to generate an Fe–H species, followed by CO_2 coordination and migratory insertion into the Fe–H bond to form an Fe formate intermediate.[99] Subsequent amine-assisted transformation affords the formamide product, while σ-bond metathesis with phenylsilane regenerates the active hydride species. A similar effect of S_8 has also been noted in related ketone hydrosilylation catalysis using the same complex.[88,100] Control experiments employing sulfur (S_8) as a free-carbene scavenger, together with spectroscopic monitoring, revealed minimal NHC dissociation, indicating that the intact NHC–Fe complex operates as the active catalyst rather than free carbene species.[99]

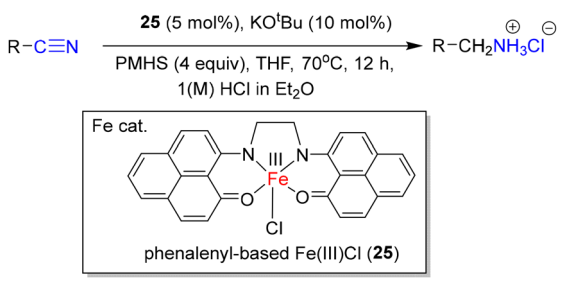

Scheme 27 Complex **25** accelerated reduction of various nitriles by using PMHS.

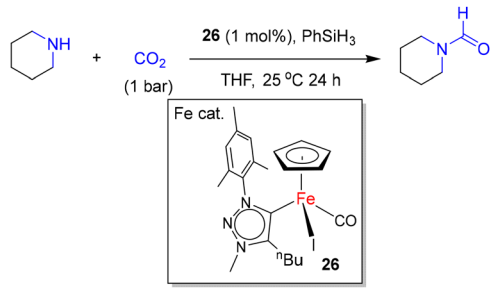

Scheme 28 Catalytic functionalization of CO_2 to formamide by using complex **26**.

An outstanding example of triazolylidene-based Fe-catalysed hydrosilylation of carbonyl compounds was reported by the Albrecht group in 2024. In this study, C,O-chelating triazolylidene ligands were synthesized and coordinated to iron to form a dimeric complex **27**, in which phenoxide ligands bridge two Fe centres. Complex **27** exhibited paramagnetic behaviour consistent with high-spin Fe(II) centres. Compared with traditional imidazolylidene systems, these triazolylidene ligands enabled remarkably high turnover numbers, reaching up to 72 000. The sterically encumbered and strongly donating triazolylidene ligands create a congested iron coordination environment that favours more substituted carbonyl substrates. This reactivity order is unusual and indicates that substrate activation is governed by catalyst–substrate interactions rather than intrinsic carbonyl electrophilicity. Ketones bearing two alkyl or aryl substituents, can engage in stronger dispersive and secondary interactions within the catalyst pocket, leading to more effective coordination and faster insertion into the Fe–H bond. In contrast, aldehydes bind less favourably due to reduced stabilizing interactions and greater conformational freedom, resulting in slower turnover (Scheme 29). The catalytic system demonstrated high efficiency and broad functional group tolerance.[101]

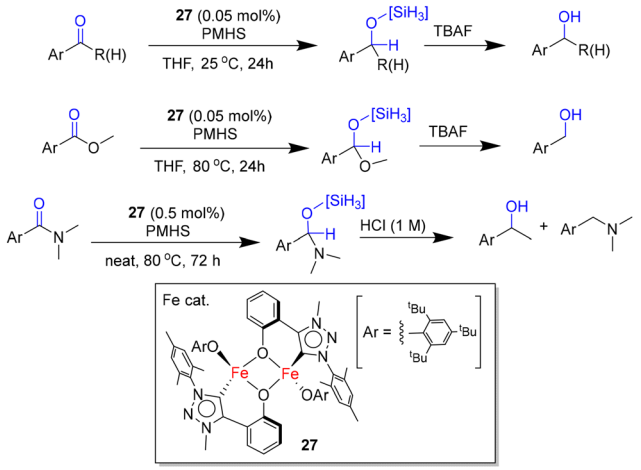

Scheme 29 Hydrosilylation of aldehydes, ketones, esters, and amides to corresponding alcohols mediated by complex **27**.

An intriguing example of Fe-catalysed hydrosilylation of carboxylic esters and carboxamides under ambient conditions was disclosed by Darcel and Zhang in 2024. An NHC ligand, IMes, was coordinated to an Fe(0) centre in the precatalyst Fe $(CO)_4$(IMes) (**28**). The IMes ligand provided strong σ-donation, stabilising the low-valent Fe centre and facilitating CO dissociation under blue LED irradiation (2 × 24 W, 450–460 nm). Among the catalysts examined, complex **28** displayed the highest catalytic efficiency for the reduction of amides to imines (Scheme 30a) and esters to alcohols (Scheme 30b) at ambient temperature. The presence of IMes not only enhanced light absorption in the blue region but also promoted the formation of a catalytically active Fe–H intermediate through Si–H bond activation of the hydrosilane. Furthermore, mechanistic investigations indicated that the IMes-bound Fe complexes remained photoactive throughout the catalytic cycle, participating in both the initial CO dissociation step and subsequent transformations, including carbonyl insertion and hydride transfer.[102]

Mechanistic studies revealed that blue light plays a dual role in the hydrosilylation mediated by complex **28**. The proposed catalytic cycle was constructed based on experimental results obtained under blue light irradiation (450–460 nm) and previous studies involving UV-light activation.[103,104] Upon initial blue light irradiation, complex **28** undergoes CO dissociation to generate $Fe(CO)_3$(IMes) (**A**), which subsequently reacts with $PhSiH_3$ to form the intermediate $Fe(H)(SiH_2Ph)(CO)_3$(IMes) (**B**). The complexes **A** and **B** were both isolated and identified. Remarkably, photo-irradiation of **B** is essential to promote the reduction of *N*,*N*-dibenzyl-4-trifluoromethylbenzamide to afford the corresponding amine. Thus, the second photoinduced CO dissociation is required to form a more reactive unsaturated Fe species that facilitates the formation of hemiaminal ether or acetal intermediate **C** without direct activation of the ester or amide carbonyl group to the Fe centre. This intermediate is then reduced in a second catalytic cycle to furnish the corresponding amine or alcohol product (Fig. 21).[102]

Darcel and Zhang further reported in 2025 that complex **28** exhibited highly efficient catalytic activity under mild con-

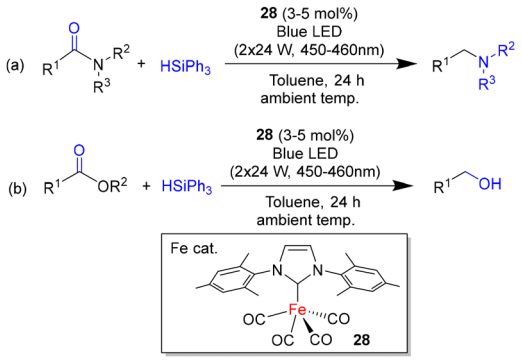

Scheme 30 Photoactive complex **28** accelerated the reduction of various nitriles and carboxylic esters by using PMHS.

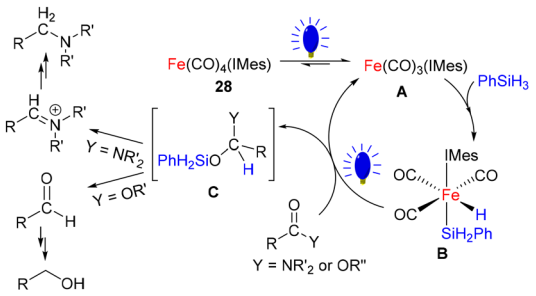

Fig. 21 Mechanistic proposal for the hydrosilylation of carboxamides and carboxylic esters by using Fe complex **28**.

ditions for the blue-light-driven hydrosilylative desulfurization of thioamides. This IMes-Fe system enabled well-organised hydrosilylation without catalyst deactivation from sulphur poisoning, which was a common issue in metal-catalysed thioamide reductions. The enhanced catalytic performance was attributed to blue-light-promoted CO ligand dissociation, facilitating the generation of active Fe species. For instance, **28** and [CpFe(IMes)(CO)$_2$][I] **29a** were effective for this reaction, whereas a different NHC ligand, ^{I}Pr, on [Fe(IPr)(CO)$_4$] **29b**, showed poorer yields (Scheme 31). The catalytic system selectively cleaved the C=S bond in tertiary thioamides to produce tertiary amines and demonstrated broad functional group tolerance, including halides, hydroxyl groups, and heteroaromatic substrates.[105]

3. Hydrosilylation by manganese complexes

Manganese's low toxicity and natural abundance make it an attractive alternative to noble metals for industrial organic synthesis, particularly in the production of fine chemicals and bulk materials.[106] The hydrosilylation of various functional groups, including relatively inert or non-polar bonds, has recently been explored using Mn catalysts.[107,108] In many modern examples, well-defined and often structurally elaborate ligand frameworks have been required to achieve efficient and selective homogeneous Mn catalysis.[108]

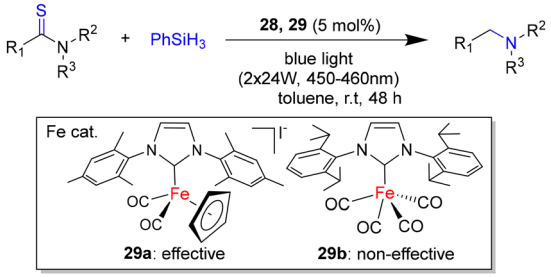

Scheme 31 Desulfurization hydrosilylation of thioamides mediated by NHC–Fe complex **28** and **29**.

As early as 1982, Yates reported the Mn-catalysed hydrosilylation of ketones under UV irradiation.[109] In 1983, Faltynek described the first Mn-catalysed alkene hydrosilylation under either UV irradiation or thermal conditions; [Mn(CO)$_5$SiPh$_3$] was employed for the hydrosilylation of 1-pentene with HMTCS-H (HMTCS = heptamethylcyclotetrasiloxane).[110] In 1987, Hilal demonstrated the hydrosilylation of 1-hexene with (EtO)$_3$SiH catalysed by [Mn$_2$(CO)$_{10}$], although the desired product was obtained in low yield.[111]

In 1990, the Cutler group reported that a Mn carbonyl complex, [(CO)$_5$MnC(O)Ph] (**I**) (Fig. 22), could catalyse the hydrosilylation of carbonyl compounds, particularly ketones.[112] In 1999, the Chung group prepared a novel class of Mn compounds, [(η^3-C$_{10}$H$_9$)Mn(CO)$_3$P(OMe)$_3$] (**J**) (Fig. 22), which were employed as pre-catalysts for the hydrosilylation of ketones.[113]

Almost a decade later, the Du group disclosed a Salen–Mn^{V} complex **K** (Fig. 22) as a precatalyst for the hydrosilylation of ketones and aldehydes, exhibiting high catalytic efficiency, low catalyst loadings, and broad functional-group tolerance. Mechanistic investigations suggested that the catalytically active species is generated *in situ via* reduction of the Mn^{V} pre-catalyst to a lower-valent Mn species under the reaction conditions, rather than direct participation of the high-valent Mn^{V} centre in the catalytic cycle.[114] Since 2014, the Trovitch group has reported Mn complexes bearing pentadentate ligands and demonstrated that (Ph$_2$PPrPDI)Mn exhibits high catalytic activity under mild conditions by using (Ph$_2$PPrPDI)Mn (**L**) (Fig. 22) for the hydrosilylation of ketones.[107] Huang and co-workers subsequently achieved the first asymmetric hydrosilylation of ketones using Mn catalysis.[115] More recently, the Gade group developed Mn complexes featuring pincer ligands, which enabled the reduction of acetophenone with moderate enantioselectivity.[116]

Beyond ketone and alkene hydrosilylation, Mn catalysis has also been extended to more challenging functional groups. To date, only a limited number of examples of Mn-catalysed amide reduction using silanes have been reported. *N*-Acetylpiperidine was readily converted to *N*-ethylpiperidine

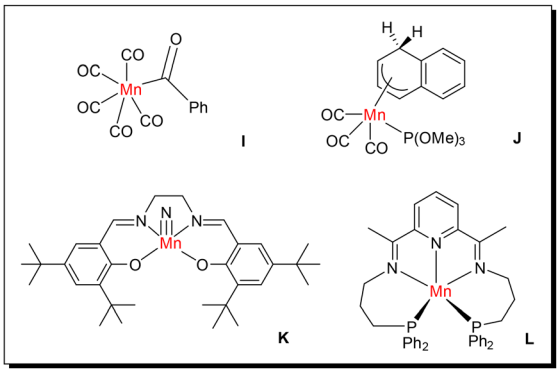

Fig. 22 Mn complexes **I**–**L** were used for hydrosilylation in reports earlier than 2018.

in the presence of a hydrosilane using [$Mn_2(CO)_{10}$] and Et_2NH.[117] Finally, the Sortais group successfully demonstrated the reduction of carboxylic acids under UV irradiation (350 nm) using hydrosilanes.[118] Collectively, these studies demonstrate the evolution of manganese hydrosilylation from photochemical carbonyl complexes to well-defined ligand-supported catalysts capable of operating under mild and selective conditions.

3.1 Hydrosilylation of alkenes and alkynes

Significant progress in Mn-catalysed alkyne hydrosilylation was reported by the Zhang group in 2019.[119] In this work, commercially available $Mn_2(CO)_{10}$ (**30**) (Scheme 32) underwent visible-light-induced homolysis to generate a radical species, $^{\bullet}Mn(CO)_5$.[120,121] This species was identified as the catalytically active intermediate and participates in hydrogen atom transfer (HAT) processes. Specifically, $^{\bullet}Mn(CO)_5$ abstracts a hydrogen atom from the silane to form the Mn hydride $HMn(CO)_5$ along with a silyl radical. The silyl radical then undergoes regioselective addition to the alkyne to generate vinyl radical intermediates **A** and **B**. Subsequent hydrogen atom transfer from $HMn(CO)_5$ to the vinyl radical affords predominantly the *E*-vinylsilane product (*E*: $R^1 > R^2$), while regenerating the active $^{\bullet}Mn(CO)_5$ species and completing the catalytic cycle. It was proposed that the stereochemical outcome is determined during the HAT step, where formation of the thermodynamically more stable *E*-configured vinylsilane (based on $R^1 > R^2$ priority) is favoured (Fig. 23). Control experiments reported in the literature supported this mechanistic proposal by indicating the involvement of radical intermediates and HAT processes.[122]

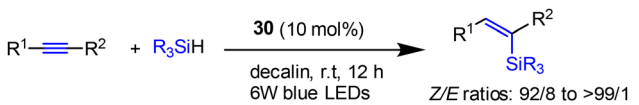

Scheme 32 Mn-catalysed *E*-selective hydrosilylation of alkynes activated by visible light using **30**. The *E*/*Z* assignment is based on the substituent priority ($R^1 > R^2$).

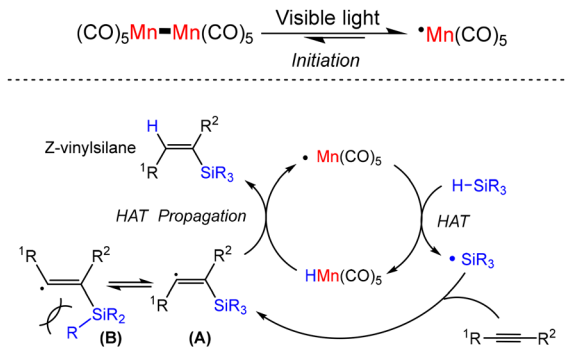

Fig. 23 Proposed mechanism for Mn-catalysed *E*-selective hydrosilylation of alkynes.

In 2021, the Xie group disclosed a Mn-catalysed dehydrosilylation of alkenes. When the catalyst precursor $Mn_2(CO)_{10}$ (**30**) was combined with appropriate ligands, the system could be directed towards either hydrosilylation or dehydrosilylation. The electron-rich bidentate phosphine iPrPNP (**L12**) significantly promoted dehydrosilylation by stabilising a key Mn–H intermediate, (**L12**)$Mn(CO)_3H$, which plays a role in hydrogen atom transfer processes and in regulating the concentration of reactive radical intermediates rather than undergoing β-hydride elimination. In contrast, JackiePhos (**L22**), a sterically demanding and electron-deficient biaryl phosphine, favoured hydrosilylation *via* a hydrogen-atom transfer (HAT) pathway, thereby enabling the formation of alkyl radical intermediates that led to the hydrosilylated products (Scheme 33). Lower olefins were required to be used under pressure, and the process exhibited broad functional-group tolerance with excellent regio- and stereoselectivity.[123]

Two ligand-controlled divergent pathways for Mn-catalysed hydrosilylation and dehydrosilylation of alkenes were proposed (Fig. 24). Thermal cleavage of $Mn_2(CO)_{10}$ (**30**) in the presence of either **L12** or **L22** initiated the reaction, generating Mn radical species **A** or **B**, respectively. Intermediate **B** reacted with silanes *via* HAT to form a Mn–H species and a silyl radical **C**,[124] which rapidly underwent radical addition to olefins **D** to generate a secondary alkyl radical **E**. The ^{iPr}PNP ligand (**L12**) facilitated the formation of (L12)$Mn(CO)_3^{\bullet}$ (**A**) and the corresponding hydride (L12)$Mn(CO)_3H$ (**H**).[125,126] This Mn–H intermediate plays a key role in regulating the concentration of the highly reactive radical **A**, maintaining a low steady-state concentration that favours the formation of intermediate **F**. Formation of the dehydrosilylation product **J** was attributed to the involvement of an alkyl-Mn(I) intermediate **F**, which readily underwent CO dissociation to form **G**, followed by *syn*-periplanar β-hydride elimination. By contrast, JackiePhos (**L22**) preferentially promoted hydrosilylation, which proceeded *via* HAT from the Mn hydride (**L22**)$Mn(CO)_4H$ (**I**) to the alkyl radical **E**, thereby affording the hydrosi-

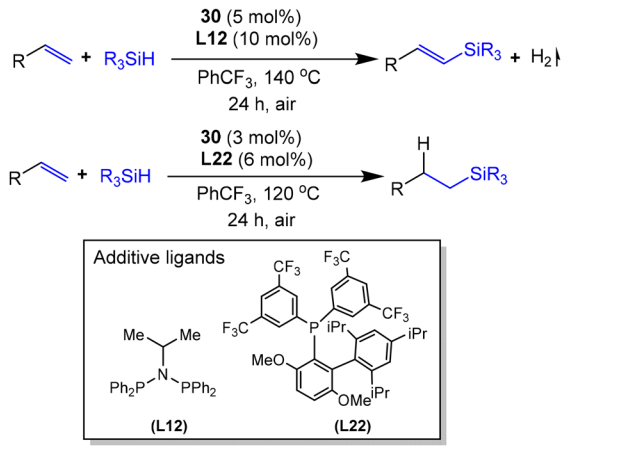

Scheme 33 Ligand-controlled Mn-catalysed hydrosilylation and divergent silylation.

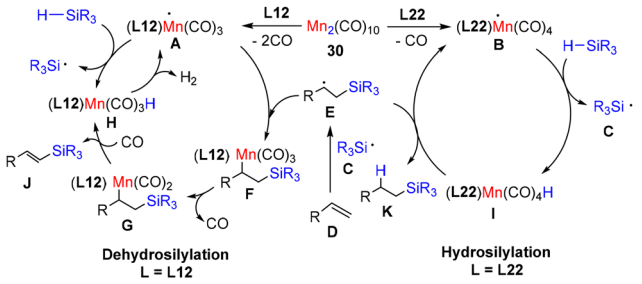

Fig. 24 Tentative mechanism for hydrosilylation and dehydrogenative silylation by complex **30** and additive ligands.

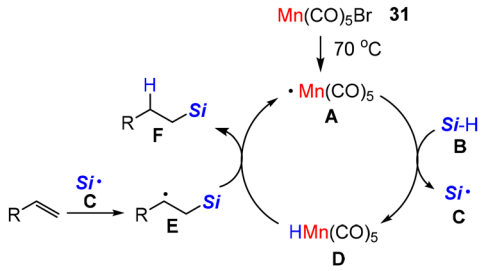

Fig. 25 Tentative mechanistic pathway for hydrosilylation of terminal alkenes using complex **31**.

lylated product **K**.[123] In addition, an equilibrium between intermediates **A** and **H**, involving reversible H_2 evolution and silyl radical formation, provides a clearer representation of the catalytic cycle.

An outstanding example of Mn-catalysed olefin hydrosilylation was reported by Thieuleux and co-workers in 2023. A ligand-free, commercially available Mn complex, [$Mn(CO)_5Br$] (**31**), was identified as a highly effective catalyst for the hydrosilylation of terminal alkenes. A broad range of alkenes was selectively hydrosilylated in an anti-Markovnikov fashion using various silanes, including industrially relevant substrates such as polymethylhydrosiloxane (PMHS) and 1,1,1,3,5,5,5-heptamethyltrisiloxane (MDHM), affording high yields without side reactions such as alkene isomerisation. The system showed remarkable tolerance to functional groups such as esters, ethers, and aromatic substituents and was operated in green solvents like anisole and even water, or under neat conditions. Also, it efficiently catalysed cross-linking of PMHS with various dienes and unsaturated esters or epoxides and formed silicone gels through Si–C or Si–O–Si bonding (Scheme 34).[127]

Mechanistic investigations indicated that hydrosilylation catalysed by complex **31** proceeds *via* a radical pathway initiated by thermal activation. Upon heating, homolytic cleavage of the Mn–Br bond in **31** generated the active Mn radical species $(CO)_5Mn^{\bullet}$ (**A**). This radical subsequently abstracted a hydrogen atom from the silane substrate **B**, producing a silyl radical **C** and a Mn hydride species, $(CO)_5Mn$–H (**D**). The generated silyl radical was added to the terminal alkene in an anti-Markovnikov manner and to give an alkyl radical intermediate **E**. This alkyl radical underwent a second hydrogen-atom transfer (HAT) from **D**, yielding the hydrosilylated product **F** and regenerating the active complex **A**, thereby completing the catalytic cycle (Fig. 25).[127]

A decent level of stereoselectivity in Mn-catalysed hydrosilylation of internal alkynes was achieved using two commercially

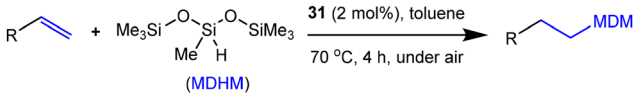

Scheme 34 Mn-catalysed hydrosilylation of terminal alkenes using complex **31** with MDHM.

available Mn complexes, the mononuclear $Mn(CO)_5Br$ (**31**) and the binuclear $Mn_2(CO)_{10}$ (**30**), as disclosed by the Li group in 2022 (Scheme 35 and Fig. 26). In the mononuclear system, a ligand such as $AsPh_3$ replaced one CO ligand to form catalytically active $MnBr(CO)_4L$ species, which mediated hydrosilylation of internal alkynes to form E-configured alkenylsilane. Conversely, the binuclear $Mn_2(CO)_{10}$ catalyst was activated with a radical initiator like LPO (lauroyl peroxide) and underwent homolytic cleavage to produce $Mn(CO)_5$ radicals, which catalysed the formation of its *Z*-isomer.[128]

They presented a mechanistic study for the hydrosilylation of internal alkyne using density functional theory (DFT) calcu-

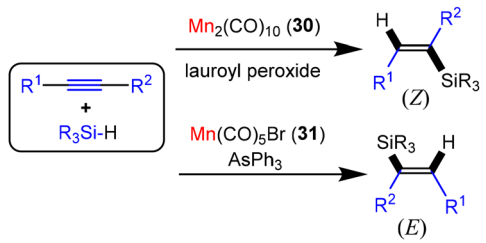

Scheme 35 Mn-catalysed stereoselective hydrosilylation of alkynes by using complexes **30** and **31**.

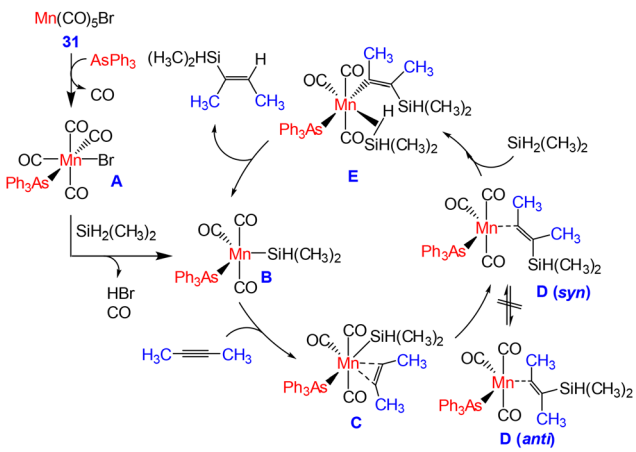

Fig. 26 Proposed mechanism for the hydrosilylation of internal alkyne by using complex **31**.

lations for complex **31** with $AsPh_3$. Initially, one CO ligand is replaced by $AsPh_3$, and subsequent CO dissociation from Mn $(CO)_4Br(AsPh_3)$ (**A**) generates the catalytically active species. Reaction with hydrosilane affords Mn-silyl intermediate **B** along with HBr formation. Coordination of the alkyne to **B** forms η^2–alkyne complex **C**, followed by migratory insertion into the Mn–Si bond to generate a Mn-vinyl intermediate. Two geometrical orientations of this intermediate were considered, namely **D**(*syn*) and **D**(*anti*), referring to the relative disposition of the Mn and silyl substituents across the newly formed C=C bond. DFT calculations indicate that formation of the Mn-(*syn*-vinyl) intermediate is energetically favoured, whereas the *anti*-isomer is disfavoured due to increased steric repulsion and higher activation barriers. Subsequent coordination of hydrosilane and hydrogen transfer leads to the release of the alkene product with the experimentally observed stereochemistry.[128]

In 2024, the Arzumanyan group proposed that $Mn_2(CO)_{10}$ (**30**) can initiate a radical-chain process as a hydrosilylation of alkenes. White-light irradiation in the presence of HFIP (HFIP = 1,1,1,3,3,3-hexafluoropropan-2-ol) enabled the system to provide alkylsilanes with anti-Markovnikov selectivity. HFIP did not coordinate directly with the Mn centre but played a key role by stabilizing radical intermediates and enhancing efficiency and selectivity. Other additives, such as trifluoroethanol, exhibited lower activity than HFIP (Scheme 36). Other metal carbonyl complexes, including $Mn(CO)_5Br$ (**31**) and $Fe(CO)_5$, were also examined but showed reduced effectiveness. The method was scalable in both batch and flow systems and was compatible with a wide range of functional groups and gaseous substrates, such as ethylene and acetylene, affording excellent yields and selectivity.[129]

Mechanistic investigations revealed that the hydrosilylation of alkenes proceeded *via* a radical autocatalytic pathway initiated by white-light irradiation. Under light irradiation, complex **30** rapidly decomposed to generate **A**. These Mn-centred radicals activated the Si–H bond, forming a silyl radical (**B**), which subsequently added to the alkene to generate a carbon-centred radical (**C**). This radical then abstracted a hydrogen atom from another Si–H group, forming the anti-Markovnikov product and regenerating **B**, thereby establishing a radical chain process (Fig. 27).[129]

In 2023, Bagh and co-workers reported the use of a specially designed tridentate N-heterocyclic carbene (NHC)–Mn complex for the hydrosilylation of terminal alkynes. The NHC ligand, featuring two picolyl (2-pyridylmethyl) donor arms, was coordinated to the Mn(I) centre in a facial N, C, N-binding mode, forming the air-stable cationic complex [Mn $(CO)_3(NHC)][PF_6]$ (**32**). Complex **32** efficiently catalysed the

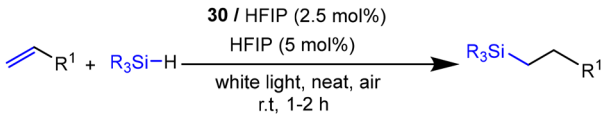

Scheme 36 Hydrosilylation of alkenes using white-light-initiated complex **30**/HFIP.

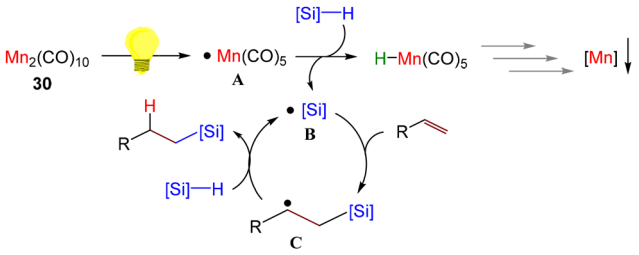

Fig. 27 Proposed mechanism for hydrosilylation of alkenes using white-light-initiated **30**/HFIP system.

hydrosilylation of terminal alkynes and favoured anti-Markovnikov addition, predominantly delivering β-(*Z*)-vinylsilanes, a synthetically valuable but thermodynamically less favoured isomer (Scheme 37).[130]

A mechanistic study was proposed for the hydrosilylation of terminal alkynes catalysed by the Mn–NHC complex **32**. According to their conclusions, complex **32** reacts with phenylsilane *via* oxidative addition of the Si–H bond to form a Mn(I)-silyl species **A**.[131] This species then coordinates the alkyne to form intermediate **B**, followed by migratory insertion into the Mn–Si bond to yield a (*Z*)-2′-silylalkenyl–Mn intermediate **C**. Owing to steric repulsion from the tridentate NHC ligand, this intermediate undergoes stereoselective isomerization through an Ojima–Crabtree-type rearrangement *via* intermediates **D** or **E**, affording the stereo-chemically more favourable *E*-configured Mn-2′-silylalkenyl intermediate **F**. Subsequent reaction with phenylsilane regenerates the active Mn-silyl species **A** and releases the *Z*-vinylsilane product (Fig. 28). This mechanism accounts for the observed regio- and stereoselectivity, leading to β-(*Z*)-vinylsilanes.[130]

In 2023, the Liu and Ke group synthesized a phenanthroline-derived tridentate (NNN-type) pincer scaffold ligand for Mn complexes **33** used for regioselective hydrosilylation of alkenes. Precisely, the complex **33a** enabled highly efficient and selective anti-Markovnikov hydrosilylation of alkenes with broad substrate tolerance under mild and solvent-free conditions. Relative studies showed that variations in the ligand framework (**33b** to **33e**) significantly affected conversion and selectivity and emphasized the importance of steric and electronic features of the ligand. For example, **33b** and **33c**, which possessed increased steric bulk, resulted in reduced catalytic

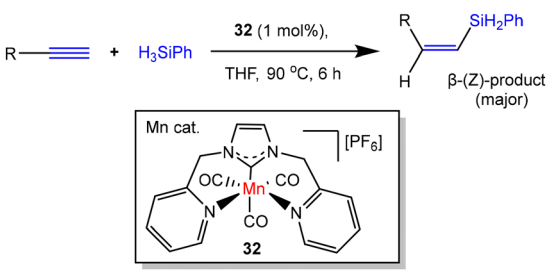

Scheme 37 Mn(I)–NHC complex **32** catalysed hydrosilylation of terminal alkynes.

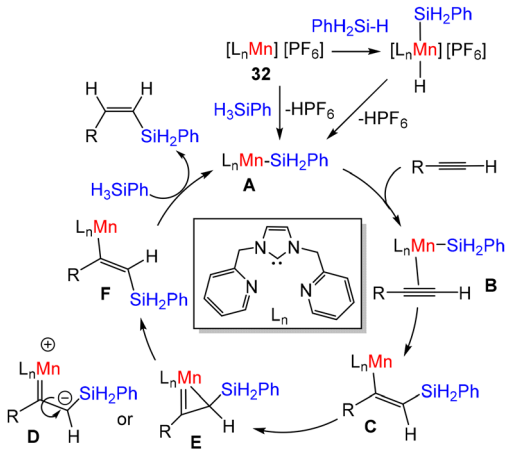

Fig. 28 Probable pathway of complex **32** for hydrosilylation of terminal alkynes.

performance, while catalysts that lacked the phenanthroline motif (**33d**, **33e**, and $MnCl_2$) showed poor or no activity. The excellent regioselectivity was driven by the preferential formation and reactivity of certain Mn alkyl intermediates, guided by the ligand's steric influence (Scheme 38).[132]

The proposed mechanistic study focused on elucidating the nature of the active species and the origin of regioselectivity. Activation of precatalyst **33a** in the presence of NaO^tBu and diphenylsilane (Ph_2SiH_2) was proposed to generate a Mn hydride species (**A**)[133–135] *in situ* (Fig. 29a). However, direct spectroscopic characterization of this hydride intermediate was not reported, and the oxidation state of manganese under catalytic conditions was inferred rather than experimentally confirmed. In the proposed cycle, hydride 1,2-insertion into the alkene affords a Mn-alkyl intermediate **B** (anti-Markovnikov), which can interconvert *via* β-hydride elimination (Fig. 29b). The divergent regioselectivity was attributed to selective σ-bond metathesis of these intermediates with Ph_2SiH_2.[132]

In 2025, Payard, Perrin and co-workers reported a mechanistic investigation of Mn-catalysed anti-Markovnikov hydrosilylation of alkenes using simple Mn(I) carbonyl precursors. Although the process required relatively high temperatures and catalyst loadings, the readily available $Mn(CO)_2Br$ (**31**) pre-

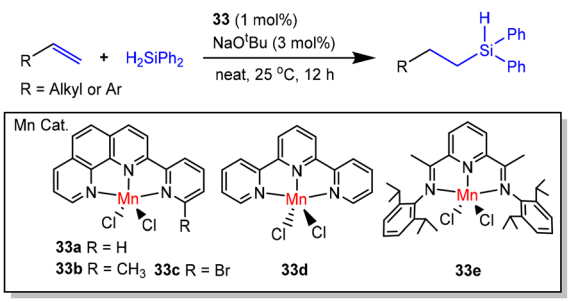

Scheme 38 Mn(I)–NHC complex **33** catalysed hydrosilylation of terminal alkynes.

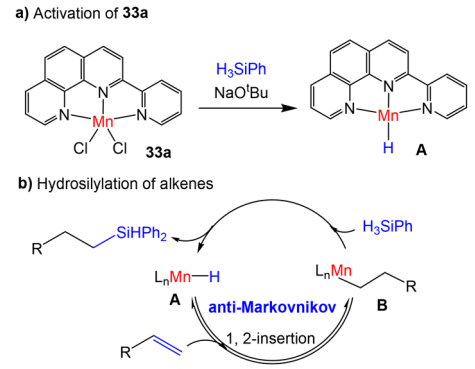

Fig. 29 Proposed mechanism for Mn-catalysed hydrosilylation of alkenes by using complex **33**.

catalyst enabled the hydrosilylation of terminal and activated alkenes with good selectivity. The study focused primarily on elucidating the nature of the active species and the origin of regioselectivity. Mechanistic investigations suggested that the data were consistent with retention of a Mn(I) manifold during catalysis. An air-stable Mn(I)-alkyl pre-catalyst, $Mn(CO)_5(n\text{-Oct})$ (**34**), was identified as a competent entry to the catalytically active species and exhibited improved reactivity compared to $Mn(CO)_2Br$ (**31**) (Scheme 39).[136] Two mechanisms—an initiation step and a catalytic cycle were proposed for the thermal hydrosilylation reaction catalysed by complex **31**, which exhibits an induction period. The catalyst is initially activated by CO dissociation from species **A**, enabling silane coordination to form intermediate **B**. Subsequent σ-bond metathesis generates the corresponding hydride species **C**, which is stabilised by coordination with the alkene substrate to form **D**. Insertion of the alkene into the Mn–H bond, followed by σ-bond metathesis with an additional silane molecule, affords intermediate **E**. This species then binds another alkene molecule to generate the catalytically key intermediate **F**. The hydrosilylation catalysis proceeds *via* successive alkene insertion, alkyl isomerisation, and σ-bond metathesis steps. These elementary transformations constitute a closed catalytic cycle that promotes selective anti-Markovnikov hydrosilylation (Fig. 30). Importantly, although Mn carbonyl complexes are frequently associated with radical pathways involving silyl radical formation under light irradiation, such a mechanism was experimentally ruled out for this thermally driven reaction.

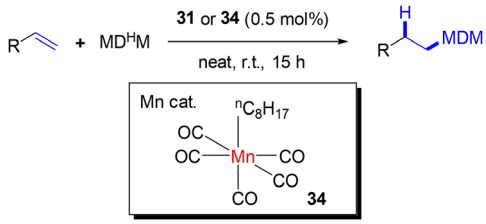

Scheme 39 Mn-catalysed anti-Markovnikov hydrosilylation of alkenes with MDHM by using complex **34**.

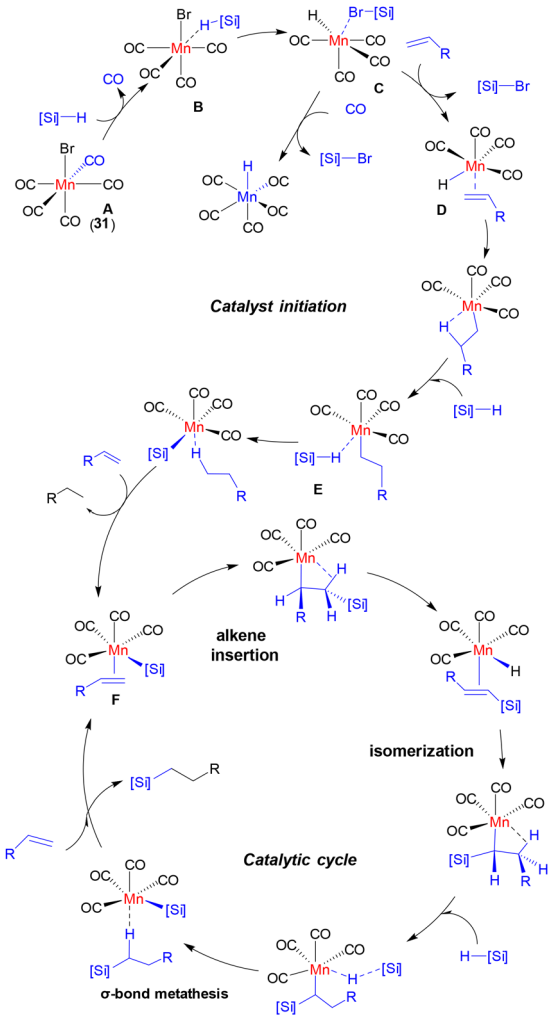

Fig. 30 Comprehensive updated mechanism for the anti-Markovnikov hydrosilylation of alkene mediated by $Mn(CO)_5Br$ (**31**).

The hydrosilylation was not inhibited by the presence of radical scavengers, and no radical-derived by-products were detected, indicating that free silyl radicals are not involved. Moreover, $Mn(CO)_5H$, often proposed as a reactive intermediate, was identified as an inactive species arising from a side reaction between complex **31** and the silane, thereby reducing overall catalytic efficiency. Notably, replacing complex **31** with an Mn(I)-alkyl pre-catalyst suppresses catalyst deactivation and provides direct access to the active catalytic cycle.[121,136]

3.2 Hydrosilylation of carbonyl compounds

In 2020, Kundu and co-workers reported a Mn(I) complex **35a–e** bearing a new bidentate NN ligand for the hydrosilylation of ketones and nitriles. These NN ligands contain a central nitrogen donor flanked by 6-methylpyridine and benzimidazole groups. The resulting complexes exhibited moderate catalytic efficiency for the monohydrosilylation of ketones, which were selectively converted into the corresponding silyl ethers, as well as for the dihydrosilylation of nitriles under mild conditions (Scheme 40). Complexes **35a**, **35b**, and **35c** showed very poor reactivity towards the reduction of acetophenone using phenylsilane, although complexes **35d** and **35e** presented a quantitative yield of the silyl ether. Notably, chemoselective reduction of carbonyl groups over olefinic bonds in carbonyl and nitrile substrates containing alkenyl groups was also observed.[137] Several control experiments indicated that radical species are involved in the hydrosilylation. In addition, ^1H NMR observation of a reaction product of **35e** with $PhSiH_3$ demonstrated the existence of a Mn–H complex or a $Mn(\eta^2$-silane) species involving η^2-Si–H coordination as an intermediate. However, more detailed mechanistic studies are necessary at this stage to clarify the catalytic cycle.

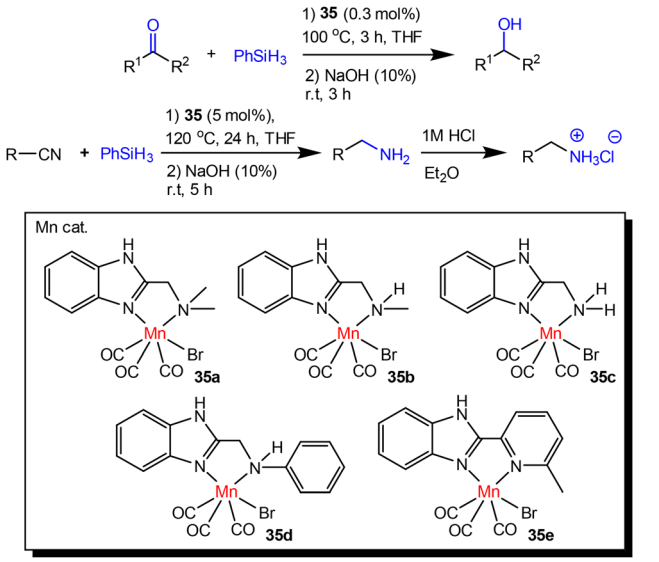

Scheme 40 Mn-catalysed hydrosilylation of ketones and nitriles by using complex **35a–e**.

In 2020, Madrahimov, Bengali and co-workers reported an example of Mn-catalysed chemoselective hydrosilylation of aldehydes. They developed a class of air-stable Mn(I) complexes bearing bulky diimine ligands, such as $[(iPr_2Ph\text{-}DAB)Mn(CO)_3Br]$ (**36a**), $[(iPr_2Ph\text{-}DAB)Mn(CO)_4]^+$ (**36b**), $[(iPr_2Ph\text{-}DAB)Mn(CO)_3(NCMe)]^+$ (**36c**), and $[(Me_2Ph\text{-}DAB)Mn(CO)_3(NCMe)]^+$ (**36d**) [R-DAB = *N*,*N*-bis(2,6-*R*)-1,4-diaza-1,3-butadiene]. These ligands provide a rigid and electronically tunable environment that facilitates efficient catalytic hydrosilylation of aldehydes, with turnover frequencies reaching up to 150 h^{-1}. The electronic characteristics of the ligands influence both the oxidative addition of the Si–H bond and the subsequent insertion of the carbonyl group into the Mn–H bond (Scheme 41). Notably, the conversion of aromatic aldehydes to the corresponding alcohols was more efficient than that of comparable aliphatic aldehydes.[138]

A well-defined PNP-Mn(I) hydride complex had been the focus of hydrosilylation of carbonyl compounds by Kirchner and co-workers in 2021. Among the tested complexes, a PNP-Mn(I) hydride complex $[Mn(PNP\text{-}iPr)(CO)_2H]$ **37** derived from a 2,6-diaminopyridine scaffold exhibited the highest cata-

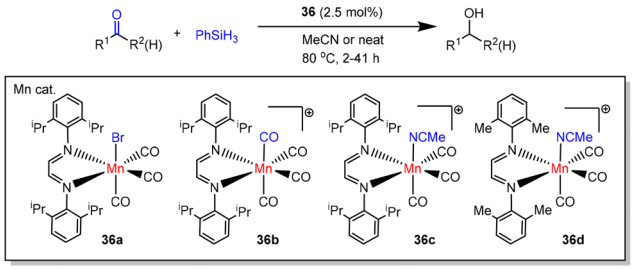

Scheme 41 Manganese α-diimine complex **36** is used for hydrosilylation of aldehydes and ketones.

lytic proficiency. The catalyst was simplified for the selective hydrosilylation of both aldehydes and ketones using PMHS as a hydride source (Scheme 42). Chemoselectivity was also shown by the system, which reduced carbonyl groups in the presence of potentially reducible functional groups, including nitriles and C=C double bonds.[139]

An outstanding novel bidentate 2-iminopyrrolyl alkyl-Mn complexes were synthesized and employed for catalytic hydrosilylation of carbonyl compounds by the group of Cruz and Gomes in 2022. They synthesized two Mn complexes, a binuclear chloride-bridged complex **38a** and a monomeric alkyl complex **38b**. Complex **38a** was converted into complex **38b** upon the alkylation with $LiCH_2SiMe_3$, which contained a (trimethylsilyl)methyl group (Scheme 43). Complex **38b** has a distorted tetrahedral geometry and showed high catalytic activity for the hydrosilylation of aldehydes and ketones under ambient conditions, with turnover frequencies up to 95 min^{-1}.[140]

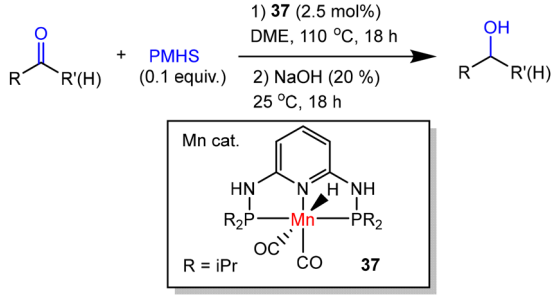

Scheme 42 Mn-catalysed hydrosilylation of ketones and aldehydes by using complex **37**.

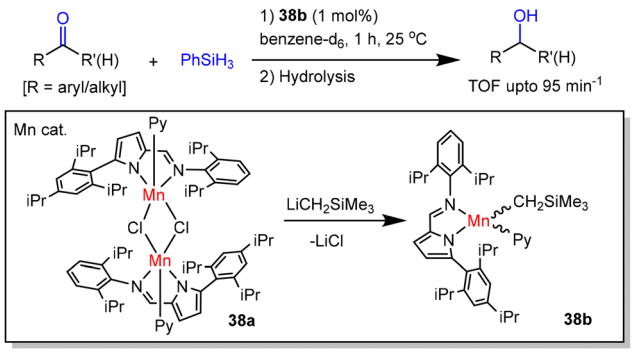

Scheme 43 Hydrosilylation of carbonyl compounds catalysed by a 2-iminopyrrolyl alkyl-Mn(II) complex **38**.

A mechanistic pathway was proposed for the hydrosilylation of carbonyl compounds catalysed by complex **38b**. Upon activation with phenylsilane ($PhSiH_3$), complex **38b** is proposed to generate a Mn(II)–hydride species *via* elimination of $(CH_3)_3SiCH_2SiH_2Ph$. Subsequent reaction with a second equivalent of silane leads to dihydrogen evolution and formation of a silyl–Mn(II) intermediate **A**. Intermediate **A** undergoes successive hydride transfer from the Si–H bond to two carbonyl groups, affording intermediates **C** and **E** in Cycle **I**. Nucleophilic attack of the resulting alkoxide on silicon generates intermediate **F**. Regeneration of **A** occurs with release of the tertiary silane $PhSiH(OCRR')_2$, consistent with experimental detection of this product rather than a monosubstituted secondary silane, which could be formed from **C**. In an alternative pathway (Cycle **II**), intermediate **F** coordinates an additional substrate molecule to form species **I**, followed by migratory insertion of the C=O group into the Mn–Si bond to yield intermediate **J**. Subsequent product dissociation from **J** releases the quaternary silane $PhSi(OCHRR')_3$ and regenerates the catalytically active Mn-silyl species **F**, thereby closing the catalytic cycle (Fig. 31).[140]

In a seminal study, a series of well-defined Mn(III)-salan (salan = *N*,*N*-dialkylated bis(salicylidene)ethylenediamine) complexes were synthesized and evaluated for hydrosilylation of carbonyl compounds by Du and co-workers in 2023. The Mn(III)-salan complexes with azide ligands, such as [(salan-tBu$_2$)Mn(N$_3$)] **39b**, showed better catalytic activity than their chloride counterparts [(salan-tBu)MnCl] **39a**. Alternatively, chloride complexes required activation by silver salts (*e.g.*, $AgClO_4$) to attain significant catalytic activity. Relative investi-

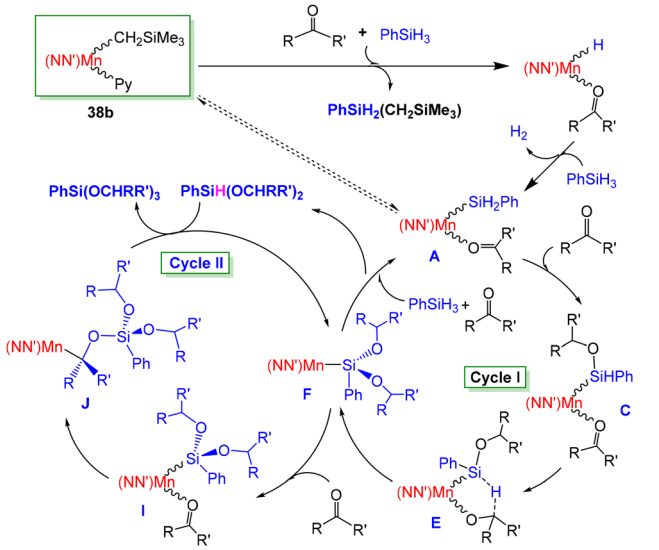

Fig. 31 Suggested catalytic cycles for carbonyl hydrosilylation by complex **38b**.

gation also presented that these salen-based Mn complexes performed better than their salen-based analogues in hydrosilylation reactions. Moreover, the catalyst could be reused for several cycles without a noticeable loss of activity, and gram-scale reactions proceeded smoothly under the solvent-free conditions (Scheme 44). The reaction selectively reduced carbonyl groups without affecting the C=C bonds, demonstrating functional group tolerance.[141]

In 2025, Matsubara and co-workers reported the synthesis and structural characterisation of a series of Mn(II) phenoxyimine complexes (**40a–40c**) bearing hemilabile pendant nitrogen donors, including pyridyl, dimethylamino, and piperidinyl groups and evaluated their catalytic activity in the hydrosilylation of aldehydes and acetophenone. These complexes efficiently catalysed the hydrosilylation of aldehydes using $PhSiH_3$ in the presence of water (Scheme 45). Control experiments demonstrated that the addition of water significantly enhanced catalytic activity. Although the precise mechanistic role of water was not fully elucidated, the authors proposed that water oxygen coordinates to Mn and subsequent deprotonation of water by the pendant nitrogen group gives Mn^{-}–OH species. The OH group on Mn can be easily converted to hydride with hydrosilane, which is active in hydrosilylation by analogy to related cobalt-catalysed system.[142] A range of aromatic and aliphatic aldehydes was converted into the corresponding alcohols after fluoride workup in moderate to excellent yields. Notably, this represents the first example of Mn(II)-catalysed, water-promoted hydrosilylation of aldehydes.[143]

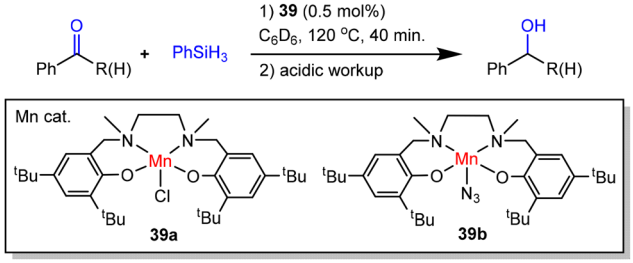

Scheme 44 Mn(III) azide-catalysed hydrosilylation of carbonyl compounds with $PhSiH_3$ by using complex **39**.

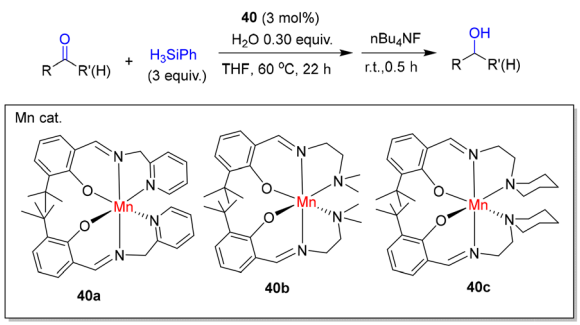

Scheme 45 Mn-catalysed hydrosilylation of aldehydes and ketones with phenylsilane by using complex **40a–c**.

In 2025, Moesch and co-workers reported the first systematic study of dinuclear Mn(I) thiopyridine complexes as efficient photocatalysts for the hydrosilylation of ketones. They synthesised and evaluated three dimeric complexes of the type $[\{Mn(6\text{-R-PyS})(CO)_3\}_2]$ (R = H, CH_3, CF_3) (**41**) under visible-light irradiation. At room temperature and with a low catalyst loading (0.1 mol%), these catalysts facilitated the hydrosilylation of both aromatic and aliphatic ketones, achieving complete conversion within 90 minutes, with optimal activity at 427 nm (Scheme 46). Further mechanistic investigations revealed an induction period and light-induced CO dissociation, generating a paramagnetic active species that remains catalytically competent in the dark but is air-sensitive. Notably, the system also performed efficiently in continuous-flow photochemistry, reducing the residence time to 14 min.[144]

3.3 Hydrosilylation of carboxylic acids and derivatives

In 2019, Werle, Leitner, and co-workers reported Mn(I) complexes **42a** and **42b** bearing triazole ligands as efficient catalysts for hydrosilylation of carbonyl and carboxyl compounds. These well-defined complexes were structurally characterised and exhibited high catalytic efficiency at loadings as low as 0.25 mol% at 80 °C, successfully converting a wide range of substrates, including ketones, esters, and carboxylic acids, into the corresponding alcohols in excellent yields (Scheme 47).[145]

They proposed a catalytic cycle for the hydrosilylation of C=O groups in carboxylic compounds. The cycle is initiated by the formation of a Mn hydride species [Mn–H],[146,147] generated from complex **42** in the presence of phenylsilane, along with the concurrent formation of a silyl cation (species **A**). Once formed, the Mn–H species transfers a hydride to the electrophilic carbonyl or carboxyl substrate, generating a silyl ether intermediate **B**, which can subsequently undergo hydrolysis or desilylation to form intermediate aldehyde **C**. This intermediate is then further reduced *via* a second Mn-catalysed hydride transfer to yield alkyl or silyl ether derivatives, which upon hydrolysis afford the corresponding alcohol **D** or ether **E** (Fig. 32). In the case of esters and carboxylic acids, the mechanism involves consecutive reduction steps, in which the carbo-

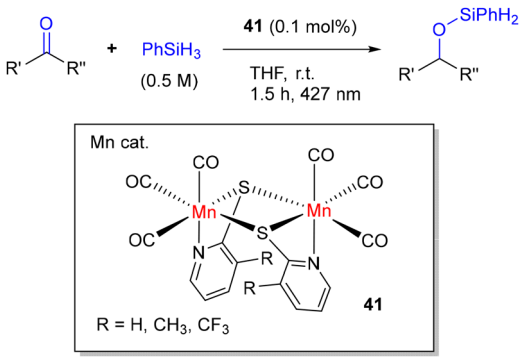

Scheme 46 Mn-catalysed hydrosilylation of ketones with phenylsilane and visible-light irradiation by using complex **41**.

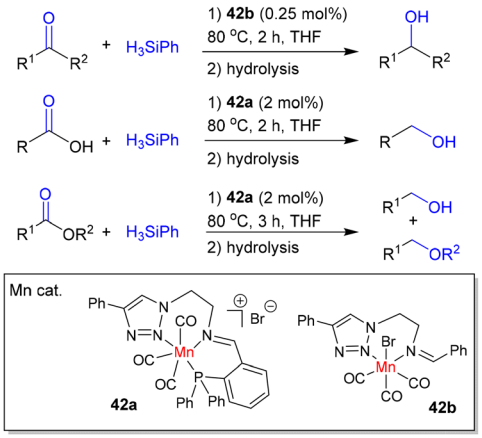

Scheme 47 Mn-catalysed hydrosilylation of ketones, esters, and carboxylic acids by using complex **42**.

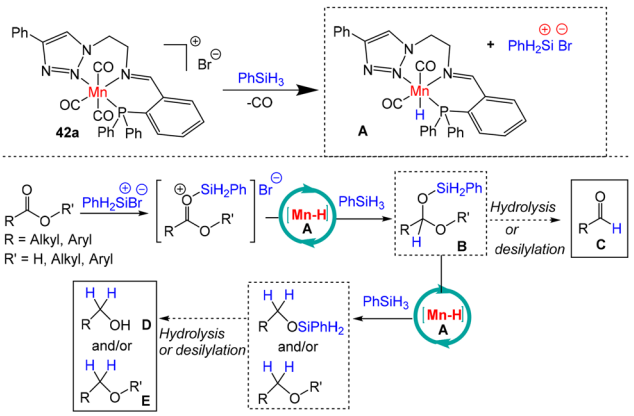

Fig. 32 A proposed mechanism for hydrosilylation of carboxylic acids or esters catalysed by Mn complex **42**.

nyl group is first converted into the corresponding aldehyde **C** and subsequently reduced to the alcohol **D**.[145]

Werle and co-workers in 2021 demonstrated hydrosilylation of alkyl and aryl carboxylic acids using the commercially available complex $[Mn(CO)_5Br]$ (**31**) and phenylsilane ($PhSiH_3$). Low catalyst loadings (≤0.5 mol%) and reduced amounts of silane were sufficient to achieve high efficiency, particularly for larger-scale applications (Scheme 48a). The complex **42a** was also examined as a catalyst under the same conditions; however, it afforded a lower yield compared to complex **31**. Signals corresponding to the free NNP ligand were detected after the reaction, indicating ligand dissociation, and no catalytic activity was observed with other PNP-type ligand frameworks. The detection of CO in the stoichiometric reactions of **31** indicated that one carbonyl ligand dissociated from **31** under the reaction conditions, resulting in an intermediate, $[Mn(CO)_4Br]$ (**A**). A key observation was the immediate evolution of hydrogen gas upon mixing $PhSiH_3$ with carboxylic acids, suggesting a dehydrogenative coupling process that forms silyl esters ($PhSiH_x(O_2CR)y$). These silyl ester intermediates are subsequently reduced to silylated alcohols, which, upon hydrolysis, yield the final alcohol products (Scheme 48b and Fig. 33).[148]

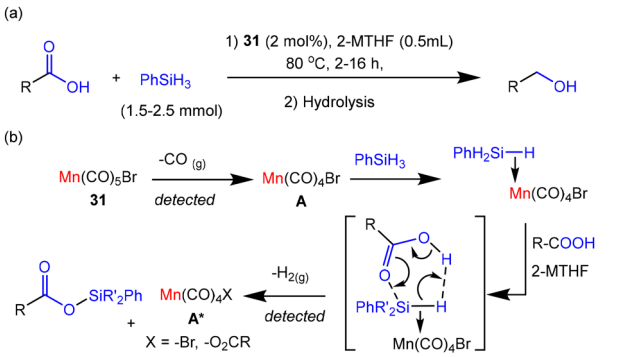

Scheme 48 (a) Mn-catalysed hydrosilylation of carboxylic acid by using complex **31** and (b) stoichiometric reactions of **31** with hydrosilane and carboxylic acid.

In 2021, García and González reported an example of Mn-catalysed hydrosilylation of carbon dioxide using $[Mn(CO)_5Br]$ (**31**). After 1 h at 50 °C under CO_2 pressure of 4 bar, triethylsilyl formate ($Et_3SiOCHO$) was obtained in 67% yield using THF as the solvent. The product selectivity and yield were further modified by changing the solvent composition to a mixture of toluene and THF, affording bis(triethylsilyl)acetal ($(Et_3SiO)_2CH_2$) in 86% yield (Scheme 49). In addition, at room temperature and atmospheric pressure, hydrosilylation of CO_2 proceeded efficiently in THF or in mixed THF/toluene solvents, resulting in high Et_3SiH conversion (92–99%), although with reduced selectivity.[149]

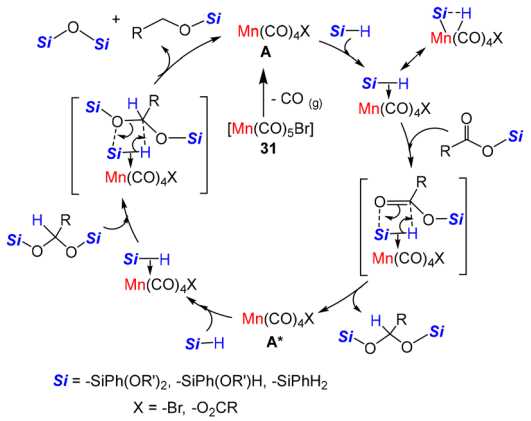

Fig. 33 Proposed mechanism for Mn-catalysed hydrosilylation of carboxylic acid by using complex **31**.

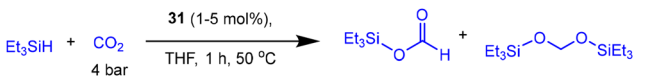

Scheme 49 Mn-catalysed hydrosilylation of carbon dioxide by using complex **31**, to silyl formate and bis(silyl)acetal.

The mechanistic study initiated with the activation of the Mn(I) pre-catalyst **31**. It was closely related to the hydrogen atom transfer (HAT) mechanism.[108,150] First, a key step involved the homolytic cleavage of the Mn–Br bond to generate Mn radical species **A**, which performed a hydrogen abstraction from triethylsilane to yield Mn-hydride **B** and silyl radical species. The silyl radical reacts with CO_2 to generate silyl-formate radical **D**. Successively, a hydrogen atom was transferred from **B** to **D**, yielding the product **E** and regenerating **A** (Fig. 34). The same hydrosilylation mechanism was followed for the reduction of the bis(silyl)acetal product.[150] For the selective hydrosilylation of alkynes in the presence of diphenylmethylsilane and dialuroyl peroxide, a radical intermediate was obtained from **B**, as reported by the Wang group in 2019.[149]

In 2020, Bagh and co-workers investigated the complex *fac*-[Mn(xantphos)(CO)$_3$Br] (**43**), bearing the bidentate bisphosphine ligand xantphos, for the hydrosilylation of esters to the corresponding alcohols (Scheme 50). The rigid chelating nature of xantphos ensured a well-defined coordination environment around the Mn centre, which was vital for the selective reduction of esters to alcohols without yielding partially reduced ethers. The reaction conditions were compatible with a wide range of aliphatic, aromatic, and cyclic esters bearing diverse functional groups, including fatty esters and polyesters, and enabled selective reduction to silyl ethers without over-reduction or interference from other reducible moieties.[151]

This study was subsequently extended by Royo and co-workers in 2020, who employed a nitrogen-heterocyclic carbene (NHC) ligand in a Mn(I) complex, [Mn(bis-NHC)(CO)$_3$Br] (**44**), for the hydrosilylation of esters to the corresponding alcohols (Scheme 51). The NHC ligand enhanced electron density at the metal centre, and improved catalytic performance in hydrosilylation reactions, allowing the Mn–NHC complex to selectively reduce esters to alcohols. Interestingly, Mn NMR spectra were recorded for the reaction mixtures, revealing the existence of three possible intermediates during the reaction, one of which was reversibly formed upon addition of hydrosilane to **44**. As no CO ligand dissociation was detected by *in situ* IR spectroscopy, an outer-sphere mechanism was proposed for the hydrosilylation catalysed by **44**.[152]

In 2021, Mandal and co-workers investigated the phosphine-free N,N,O-PLY ligand, which was specifically designed for coordination to Mn(I) and formed complex **45** that catalysed the reduction of esters to corresponding alcohols by using PMHS as a hydrosilane source (Scheme 52). The ligand exhibited hemilability with only the nitrogen atoms coordinating to the Mn centre that enabled a single-electron transfer (SET) process, as observed in the other systems using Mn(I) catalysts. A wide range of esters, including aromatic, aliphatic, cyclic, and complex molecules, were efficiently converted to their corresponding alcohols in satisfactory to excellent yields.[153]

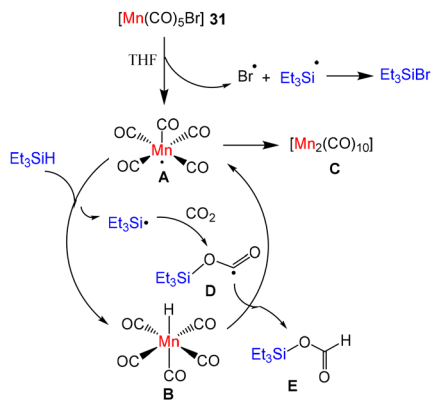

Fig. 34 Proposed mechanism for the hydrosilylation of CO_2 by using Mn-complex **31**.

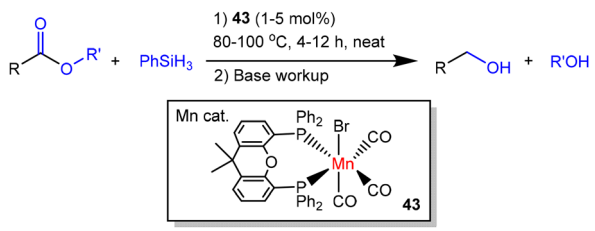

Scheme 50 Hydrosilylation of esters by dippe-Mn complex **43** to corresponding alcohols.

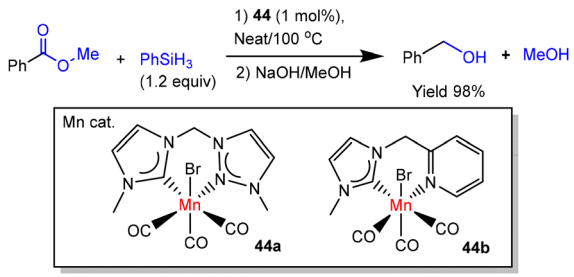

Scheme 51 NHC–Mn complex **44** is used for the reduction of esters to corresponding alcohols.

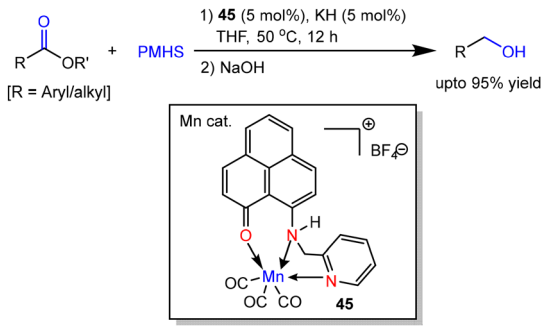

Scheme 52 Mn-catalysed hydrosilylation of esters by using complex **45**.

They proposed that the Mn(I) pre-catalyst **45**, upon treatment with potassium hydride, undergoes one-electron reduction to form a PLY-based radical species **A**, which initiates the cycle with the SET processes. This radical species cleaves the Si–H bond of PMHS and generates a silyl radical and an Mn(I)–H species **B**.[145] Succeeding, the catalytic cycle involved **B** and transferred the hydride to the carbonyl carbon of the ester, followed by radical recombination with the silyl radical to form the silyl ether **C**.[154–156] This process regenerated the radical catalyst **A** by single-electron transfer back to the catalyst (Fig. 35). Yet again, the silyl ether **C** took part in the second catalytic cycle, when a second hydride was transferred to the carbon centre to produce the silylated product **D**, which, upon hydrolysis, yielded the corresponding alcohol. The silyl radical from the second cycle was predicted to form a silyl ether **E** as the byproduct.[153]

In 2019, Mandal and co-workers reported an efficient Mn-catalysed hydrosilylation of primary amides. They employed Mn(III) complex **46** bearing a tetracoordinated phenalenyl-based ligand as a catalyst precursor. The design of complex **46** provided both electronic and steric control, facilitated the activation of Si–H bonds in the presence of KO^{t}Bu, and enabled efficient hydrosilylation of primary amides into primary amines (Scheme 53). Interestingly, the system could selectively convert primary amides into the corresponding intermediates, nitriles, in the presence of secondary amides, such as *N*-benzylamide, which remained intact.[157]

A mechanistic pathway was proposed for the hydrosilylation of primary amides to either nitriles or amines (Fig. 36). Initially, precatalyst **46** reacts with KO^{t}Bu to generate an alkoxide complex **A**.[158] Subsequent reaction of **A** with $PhSiH_3$ leads to the abstraction of the alkoxide ligand and formation of a cationic Mn species **B**, which is proposed to be the catalytically active intermediate.[159] Coordination of the primary amide occurs at this cationic Mn centre through a vacant coordination site, assisted by hydrogen bonding between the N–H moiety of the substrate and the ligand oxygen atom, affording intermediate **C**. Although structural analysis of precatalyst **46** demonstrated that the Mn centre is capable of interacting with amide substrates, the catalytically relevant binding event is proposed to occur from the cationic intermediate **B** rather than from the neutral precatalyst. Dehydrogenative conversion of the coordinated amide leads to nitrile formation with concomitant evolution of H_2, regenerating the cationic Mn species and affording a nitrile-coordinated intermediate. Subsequent hydrosilylative reduction of the nitrile *via* an imine intermediate furnishes the corresponding amine. In the presence of a secondary amide, preferential coordination to the cationic Mn centre inhibits binding and further reduction of the nitrile intermediate, thereby resulting in selective nitrile formation.[157]

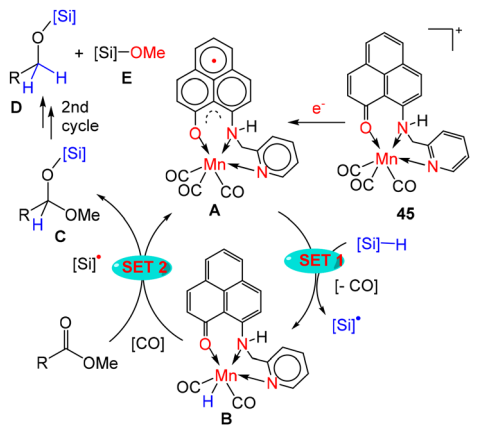

Fig. 35 Possible mechanism for SET-facilitated ester hydrosilylation with **45** using PMHS.

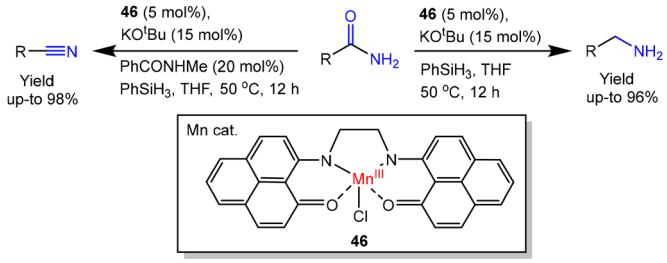

Scheme 53 Dual activity by Mn complex **46** in the hydrosilylation of amides into amine or nitrile.

3.4 Hydrosilylation of other compounds

In 2022, Bagh and co-workers reported a well-defined, air-stable Mn(II) complex (**47**) bearing an NNO pincer ligand for the chemoselective hydrosilylation of nitroarenes to aromatic amines (Scheme 54). The complex was structurally characterised as a Mn(II) species, and the catalytically active intermediate is proposed to be generated from this Mn(II) precatalyst under the reaction conditions. A wide range of nitroarenes bearing electron-withdrawing and electron-donating substituents was efficiently reduced with good functional group tolerance, including amides, esters, halides, and alkenes, thereby demonstrating the high chemoselectivity of the system.

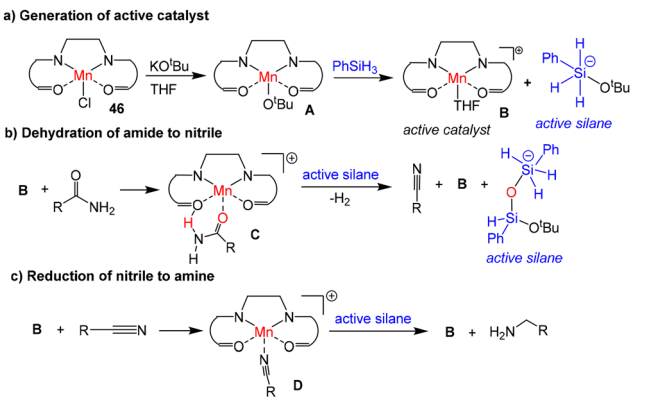

Fig. 36 Suggested pathway for Mn-catalysed reduction of primary amides by using complex **46**.

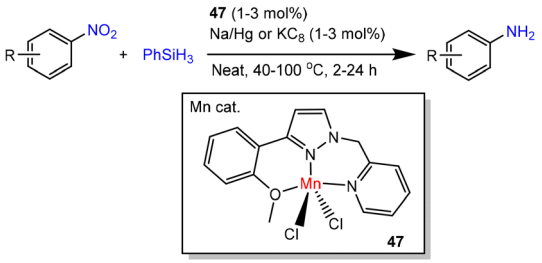

Scheme 54 Hydrosilylation of nitroarenes by Mn(II)–NNO pincer complex **47**.

Notably, other potentially reducible functional groups remained intact in many cases, highlighting the selectivity imparted by the ligand environment. Although detailed mechanistic investigations were not reported to establish the oxidation states of the Mn centre during catalysis, the transformation is proposed to proceed *via* Mn-based intermediates, plausibly involving the formation of a Mn–H species. This study represents the first example of Mn-catalysed hydrosilylation of nitroarenes and underscores the important role of the NNO ligand framework in achieving efficient and selective reductions.[160]

4. Conclusions

Over the past few decades, Fe- and Mn-catalysed hydrosilylation has advanced substantially, driven by the development of diverse metal–ligand architectures and the expansion of substrate scope. Early studies in the 1970s and 1980s demonstrated that simple Fe and Mn carbonyl complexes could catalyse the addition of silanes to carbonyl compounds and alkenes, although with limited activity and selectivity. Subsequently, the design of well-defined complexes incorporating phosphine, pincer, N-heterocyclic carbene, and nitrogen-based ligands enabled improved control over reactivity and selectivity. The introduction of chiral Fe and Mn catalysts further enabled enantioselective transformations, including the reduction of carbonyl compounds, olefins, and nitroarenes under comparatively mild conditions. These advances have led to catalytic systems exhibiting high chemoselectivity and broad functional group tolerance. In addition to standard transformations, Fe- and Mn-based catalysts have been applied to more challenging reductions, including carboxylic acids, esters, amides, and carbon dioxide. Control over chemo-, regio-, and enantioselectivity is achieved through careful tuning of ligand environments and reaction conditions, allowing the efficient synthesis of value-added products using readily available hydrosilanes under environmentally benign conditions. Notably, several systems display high activity at low catalyst loadings, in some cases under solvent-free conditions, particularly when supported by pincer or multidentate ligand frameworks.

A unifying feature emerging from recent studies is that the most efficient Fe- and Mn-based hydrosilylation catalysts are predominantly based on d^6 electronic configurations, particularly Fe(II) and Mn(I) complexes. These systems commonly operate *via* inner-sphere mechanisms involving metal–hydride intermediates, which play a central role in substrate activation and hydride transfer. This mechanistic insight provides a useful framework for understanding catalytic performance and for guiding the rational design of next-generation catalysts based on earth-abundant metals. Overall, the progression from early, poorly defined systems to well-designed, highly selective catalysts underscores the increasing relevance of base-metal-catalysed hydrosilylation in modern organic synthesis. Continued developments are expected to further improve the sustainability, efficiency, and practical applicability of these transformations across pharmaceuticals, fine chemicals, and materials science.

Conflicts of interest

The authors have no conflicts to declare.

Data availability

Data sharing is not applicable to this article as no new datasets were generated or analyzed in this perspective.

References

1 P. J. Chirik, *Acc. Chem. Res.*, 2015, **48**, 1687–1695.
2 R. H. Crabtree, *Chem. Rev.*, 2012, **112**, 1536–1554.
3 K. Yamamoto, T. Hayashi and M. Kumada, *J. Organomet. Chem.*, 1973, **54**, C45–C47.
4 B. Cornils and W. A. Herrmann, *J. Catal.*, 2003, **216**, 23–31.
5 K. Yamamoto, T. Hayashi and M. Kumada, *J. Organomet. Chem.*, 1972, **46**, C65–C67.
6 C. Bolm, J. Legros, J. Le Paih and L. Zani, *Chem. Rev.*, 2004, **104**, 6217–6254.
7 R. H. Morris, *Acc. Chem. Res.*, 2015, **48**, 1494–1502.
8 R. H. Morris, *Chem. Soc. Rev.*, 2009, **38**, 2282–2291.
9 K. Das, S. Waiba, A. Jana and B. Maji, *Chem. Soc. Rev.*, 2022, **51**, 4386–4464.
10 B. Maji and M. K. Barman, *Synthesis*, 2017, 3377–3393.
11 A. Gómez-Suárez, Y. Oonishi, S. Meiries and S. P. Nolan, *Organometallics*, 2013, **32**, 1106–1111.
12 M. Garbe, K. Junge and M. Beller, *Eur. J. Org. Chem.*, 2017, 4344–4362.
13 W. Liu and J. T. Groves, *Acc. Chem. Res.*, 2015, **48**, 1727–1735.
14 H.-U. Blaser, F. Spindler and M. Studer, *Appl. Catal., A*, 2001, **221**, 119–143.
15 H.-U. Blaser and M. Studer, *Appl. Catal., A*, 1999, **189**, 191–204.

16 A. Maity and T. S. Teets, *Chem. Rev.*, 2016, **116**, 8873–8911.
17 G. W. Gribble, *J. Chem. Soc., Perkin Trans. 1*, 2000, 1045–1075.
18 D. Tröegel and J. Stöhrer, *Coord. Chem. Rev.*, 2011, **255**, 1440–1459.
19 S. Pandey, K. V. Raj, D. R. Shinde, K. Vanka, V. Kashyap, S. Kurungot, C. Vinod and S. H. Chikkali, *J. Am. Chem. Soc.*, 2018, **140**, 4430–4439.
20 M. Bhunia, P. Sreejyothi and S. K. Mandal, *Coord. Chem. Rev.*, 2020, **405**, 213110.
21 B. Li, J.-B. Sortais and C. Darcel, *RSC Adv.*, 2016, **6**, 57603–57625.
22 M. Oestreich, *Angew. Chem., Int. Ed.*, 2016, **55**, 494–499.
23 T. K. Meister, K. Riener, P. Gigler, J. R. Stöhrer, W. A. Herrmann and F. E. Kühn, *ACS Catal.*, 2016, **6**, 1274–1284.
24 A. Suzuki, *J. Organomet. Chem.*, 1999, **576**, 147–168.
25 X. Lu, *Top. Catal.*, 2005, **35**, 73–86.
26 M. E. O'Reilly, S. Dutta and A. S. Veige, *Chem. Rev.*, 2016, **116**, 8105–8145.
27 L. D. de Almeida, H. Wang, K. Junge, X. Cui and M. Beller, *Angew. Chem., Int. Ed.*, 2021, **60**, 550–565.
28 W. D. Jones and R. G. Bergman, *J. Am. Chem. Soc.*, 1979, **101**, 5447–5449.
29 L. Sommer, E. Pietrusza and F. Whitmore, *J. Am. Chem. Soc.*, 1947, **69**, 188.
30 J. L. Speier, J. A. Webster and G. H. Barnes, *J. Am. Chem. Soc.*, 1957, **79**, 974–979.
31 M. F. Lappert and F. P. Scott, *J. Organomet. Chem.*, 1995, **492**, C11–C13.
32 J. V. Obligacion and P. J. Chirik, *Nat. Rev. Chem.*, 2018, **2**, 15–34.
33 D. Wang and D. Astruc, *Chem. Soc. Rev.*, 2017, **46**, 816–854.
34 C. C. Lu, T. Weyhermüller, E. Bill and K. Wieghardt, *Inorg. Chem.*, 2009, **48**, 6055–6064.
35 H. Brunner and K. Fisch, *J. Organomet. Chem.*, 1991, **412**, C11–C13.
36 N. Ahmed, *J. Organomet. Chem.*, 2024, **1009**, 123071.
37 L. Alig, M. Fritz and S. Schneider, *Chem. Rev.*, 2018, **119**, 2681–2751.
38 J. C. Ott, D. Bürgy, H. Guan and L. H. Gade, *Acc. Chem. Res.*, 2022, **55**, 857–868.
39 J. Peng and S. P. Thomas, *Synlett*, 2020, 1140–1146.
40 H. Brunner and K. Fisch, *Angew. Chem., Int. Ed. Engl.*, 1990, **29**, 1131–1132.
41 T. T. Metsänen, D. Gallego, T. Szilvási, M. Driess and M. Oestreich, *Chem. Sci.*, 2015, **6**, 7143–7149.
42 K. Kamata, A. Suzuki, Y. Nakai and H. Nakazawa, *Organometallics*, 2012, **31**, 3825–3828.
43 D. Bézier, G. T. Venkanna, L. C. M. Castro, J. Zheng, T. Roisnel, J.-B. Sortais and C. Darcel, *Adv. Synth. Catal.*, 2012, **354**, 1879–1884.
44 L. C. M. Castro, J.-B. Sortais and C. Darcel, *Chem. Commun.*, 2012, **48**, 151–153.
45 K. Junge, B. Wendt, S. Zhou and M. Beller, *Eur. J. Org. Chem.*, 2013, 2061–2065.
46 D. Peng, Y. Zhang, X. Du, L. Zhang, X. Leng, M. D. Walter and Z. Huang, *J. Am. Chem. Soc.*, 2013, **135**, 19154–19166.
47 X. Frogneux, O. Jacquet and T. Cantat, *Catal. Sci. Technol.*, 2014, **4**, 1529–1533.
48 H. Li, M. Achard, C. Bruneau, J.-B. Sortais and C. Darcel, *RSC Adv.*, 2014, **4**, 25892–25897.
49 Z. Zuo, L. Zhang, X. Leng and Z. Huang, *Chem. Commun.*, 2015, **51**, 5073–5076.
50 J. Chen, B. Cheng, M. Cao and Z. Lu, *Angew. Chem., Int. Ed.*, 2015, **54**, 4661–4664.
51 T. Bleith and L. H. Gade, *J. Am. Chem. Soc.*, 2016, **138**, 4972–4983.
52 F. S. Wekesa, R. Arias-Ugarte, L. Kong, Z. Sumner, G. P. McGovern and M. Findlater, *Organometallics*, 2015, **34**, 5051–5056.
53 M.-Y. Hu, Q. He, S.-J. Fan, Z.-C. Wang, L.-Y. Liu, Y.-J. Mu, Q. Peng and S.-F. Zhu, *Nat. Commun.*, 2018, **9**, 221.
54 A. Saini, C. R. Smith, F. S. Wekesa, A. K. Helms and M. Findlater, *Org. Biomol. Chem.*, 2018, **16**, 9368–9372.
55 Á. Raya-Barón, C. P. Galdeano-Ruano, P. Oña-Burgos, A. Rodríguez-Diéguez, R. Langer, R. López-Ruiz, R. Romero-González, I. Kuzu and I. Fernández, *Dalton Trans.*, 2018, **47**, 7272–7281.
56 B. Cheng, W. Liu and Z. Lu, *J. Am. Chem. Soc.*, 2018, **140**, 5014–5017.
57 M.-Y. Hu, J. Lian, W. Sun, T.-Z. Qiao and S.-F. Zhu, *J. Am. Chem. Soc.*, 2019, **141**, 4579–4583.
58 M.-Y. Hu, P. He, T.-Z. Qiao, W. Sun, W.-T. Li, J. Lian, J.-H. Li and S.-F. Zhu, *J. Am. Chem. Soc.*, 2020, **142**, 16894–16902.
59 P. He, M.-Y. Hu, J.-H. Li, T.-Z. Qiao, Y.-L. Lu and S.-F. Zhu, *Natl. Sci. Rev.*, 2024, **11**, nwad324.
60 P. He, M. H. Guan, M. Y. Hu, Y. J. Zhou, M. Y. Huang and S. F. Zhu, *Angew. Chem.*, 2024, **136**, e202402044.
61 C. Chen, H. Wang, Y. Sun, J. Cui, J. Xie, Y. Shi, S. Yu, X. Hong and Z. Lu, *iScience*, 2020, **23**, 101015.
62 P. W. Smith, Y. Dong and T. D. Tilley, *Chem. Sci.*, 2020, **11**, 7070–7075.
63 M. E. Fasulo, M. C. Lipke and T. D. Tilley, *Chem. Sci.*, 2013, **4**, 3882–3887.
64 B. V. Mork and T. D. Tilley, *J. Am. Chem. Soc.*, 2004, **126**, 4375–4385.
65 M. C. Lipke, A. L. Liberman-Martin and T. D. Tilley, *Angew. Chem., Int. Ed.*, 2017, **56**, 2260–2294.
66 M. C. Lipke and T. D. Tilley, *J. Am. Chem. Soc.*, 2014, **136**, 16387–16398.
67 M. C. Lipke and T. D. Tilley, *J. Am. Chem. Soc.*, 2011, **133**, 16374–16377.
68 M. Kamitani, K. Yujiri and H. Yuge, *Organometallics*, 2020, **39**, 3535–3539.
69 M. Kamitani, H. Kusaka and H. Yuge, *Chem. Lett.*, 2019, **48**, 1196–1198.
70 Y. C. Lam, R. J. Nielsen, W. A. Goddard and A. K. Dash, *Dalton Trans.*, 2017, **46**, 12507–12515.

71 Z. Guo, H. Wen, G. Liu and Z. Huang, *Org. Lett.*, 2021, **23**, 2375–2379.
72 Ł. Banach, D. Brykczyńska, A. Gorczyński, B. Wyrzykiewicz, M. Skrodzki and P. Pawluć, *Chem. Commun.*, 2022, **58**, 13763–13766.
73 W. Sun, M.-P. Li, L.-J. Li, Q. Huang, M.-Y. Hu and S.-F. Zhu, *Chem. Sci.*, 2022, **13**, 2721–2728.
74 W. Sun, M. Y. Hu, Z. S. Lu, M. Y. Huang, X. Y. Zhang and S. F. Zhu, *Angew. Chem., Int. Ed.*, 2023, **62**, e202315473.
75 A. Sen, T. Tewari, R. Kumar, C. Vinod, H. Sharma, K. Vanka and S. H. Chikkali, *Catal. Sci. Technol.*, 2024, **14**, 2752–2760.
76 N. G. Simonian, M. Féo, C. Tanguy, C. Troufflard and G. Lefèvre, *ACS Catal.*, 2024, **14**, 12163–12172.
77 X. Xie, X. Zhang, W. Gao, C. Meng, X. Wang and S. Ding, *Commun. Chem.*, 2019, **2**, 101.
78 I. Ojima, N. Clos, R. J. Donovan and P. Ingallina, *Organometallics*, 1990, **9**, 3127–3133.
79 K. A. Brady and T. A. Nile, *J. Organomet. Chem.*, 1981, **206**, 299–304.
80 C. Pradhan, S. Dubey, P. P. Samal, S. Krishnamurty and B. Punji, *Catal. Sci. Technol.*, 2025, **15**, 6716–6725.
81 H. Schratzberger and K. Kirchner, *ChemCatChem*, 2025, **17**, e202401398.
82 A. M. Schroeder and M. S. Wrighton, *J. Organomet. Chem.*, 1977, **128**, 345–358.
83 X. Wang, J. Zhao, D. Wang, L. Deng and Z. Lu, *Nat. Commun.*, 2025, **16**, 4338.
84 J. Guo, Z. Cheng, J. Chen, X. Chen and Z. Lu, *Acc. Chem. Res.*, 2021, **54**, 2701–2716.
85 B. Cheng, P. Lu, H. Zhang, X. Cheng and Z. Lu, *J. Am. Chem. Soc.*, 2017, **139**, 9439–9442.
86 G. Fan, Z. Shang, R. Li, S. Shafiei-Haghighi, Q. Peng, M. Findlater and X. Xu, *Organometallics*, 2019, **38**, 4105–4114.
87 G. Chang, P. Zhang, W. Yang, S. Xie, H. Sun, X. Li, O. Fuhr and D. Fenske, *Dalton Trans.*, 2020, **49**, 9349–9354.
88 P. V. Nylund, N. C. Ségaud and M. Albrecht, *Organometallics*, 2021, **40**, 1538–1550.
89 X. Du, X. Qi, K. Li, X. Li, H. Sun, O. Fuhr and D. Fenske, *Appl. Organomet. Chem.*, 2021, **35**, e6286.
90 K. Lou, Q. Zhou, Q. Wang, X. Fan, X. Xu and C. Cui, *Dalton Trans.*, 2021, **50**, 11016–11020.
91 C. V. Thompson, H. D. Arman and Z. J. Tonzetich, *Organometallics*, 2022, **41**, 430–440.
92 K. Matsubara, Y. Yamada, H. Iwasaki, H. Ikeda, Y. Kanetsugu, S. Kawata and Y. Koga, *Dalton Trans.*, 2023, **52**, 572–582.
93 T. Tannoux, L. Mazaud, T. Cheisson, N. Casaretto and A. Auffrant, *Dalton Trans.*, 2023, **52**, 12010–12019.
94 R. Ishii, M. Nakagawa, Y. Wada and Y. Sunada, *Dalton Trans.*, 2023, **52**, 15124–15130.
95 R. Ishii and Y. Sunada, *Dalton Trans.*, 2024, **53**, 1421–1424.
96 N. Khamis, G. J. Clarkson, S. Habershon and M. Wills, *Organometallics*, 2025, **44**, 1267–1275.
97 S. R. Tamang, A. F. Cozzolino and M. Findlater, *Org. Biomol. Chem.*, 2019, **17**, 1834–1838.
98 S. Das, H. S. Das, B. Singh, R. K. Haridasan, A. Das and S. K. Mandal, *Inorg. Chem.*, 2019, **58**, 11274–11278.
99 P. V. Nylund, G. Rigoni and M. Albrecht, *Organometallics*, 2023, **42**, 1740–1745.
100 C. Chen, Q. Xia, H. Qiu and W. Chen, *J. Organomet. Chem.*, 2015, **775**, 103–108.
101 W. Stroek, N. A. Rowlinson, M. Keilwerth, D. M. Pividori, K. Meyer and M. Albrecht, *Organometallics*, 2024, **43**, 1386–1392.
102 Q. Zhang and C. Darcel, *Eur. J. Org. Chem.*, 2024, e202400475.
103 T. Dombray, C. Helleu, C. Darcel and J. B. Sortais, *Adv. Synth. Catal.*, 2013, **355**, 3358–3362.
104 M. Bhunia, P. K. Hota, G. Vijaykumar, D. Adhikari and S. K. Mandal, *Organometallics*, 2016, **35**, 2930–2937.
105 Q. Zhang and C. Darcel, *Eur. J. Org. Chem.*, 2025, e202500048.
106 J. R. Carney, B. R. Dillon and S. P. Thomas, *Eur. J. Org. Chem.*, 2016, 3912–3929.
107 T. K. Mukhopadhyay, M. Flores, T. L. Groy and R. J. Trovitch, *J. Am. Chem. Soc.*, 2014, **136**, 882–885.
108 X. Yang and C. Wang, *Chem. – Asian J.*, 2018, **13**, 2307–2315.
109 R. L. Yates, *J. Catal.*, 1982, **78**, 111–115.
110 S. L. Pratt and R. A. Faltynek, *J. Organomet. Chem.*, 1983, **258**, C5–C8.
111 H. S. Hilal, M. Abu-Eid, M. Al-Subu and S. Khalaf, *J. Mol. Catal. A: Chem.*, 1987, **39**, 1–11.
112 P. K. Hanna, B. T. Gregg and A. R. Cutler, *Organometallics*, 1991, **10**, 31–33.
113 S. U. Son, S.-J. Paik, I. S. Lee, Y.-A. Lee, Y. K. Chung, W. K. Seok and H. N. Lee, *Organometallics*, 1999, **18**, 4114–4118.
114 V. K. Chidara and G. Du, *Organometallics*, 2013, **32**, 5034–5037.
115 X. Ma, Z. Zuo, G. Liu and Z. Huang, *ACS Omega*, 2017, **2**, 4688–4692.
116 J. Wenz, V. Vasilenko, A. Kochan, H. Wadepohl and L. H. Gade, *Eur. J. Inorg. Chem.*, 2017, 5545–5556.
117 M. Igarashi and T. Fuchikami, *Tetrahedron Lett.*, 2001, **42**, 1945–1947.
118 J. Zheng, S. Chevance, C. Darcel and J.-B. Sortais, *Chem. Commun.*, 2013, **49**, 10010–10012.
119 H. Liang, Y.-X. Ji, R.-H. Wang, Z.-H. Zhang and B. Zhang, *Org. Lett.*, 2019, **21**, 2750–2754.
120 P. Nuhant, M. S. Oderinde, J. Genovino, A. Juneau, Y. Gagné, C. Allais, G. M. Chinigo, C. Choi, N. W. Sach and L. Bernier, *Angew. Chem., Int. Ed.*, 2017, **56**, 15309–15313.
121 X. Yang and C. Wang, *Angew. Chem., Int. Ed.*, 2018, **57**, 935–940.
122 D. P. Curran and W. Shen, *J. Am. Chem. Soc.*, 1993, **115**, 6051–6059.
123 J. Dong, X.-A. Yuan, Z. Yan, L. Mu, J. Ma, C. Zhu and J. Xie, *Nat. Chem.*, 2021, **13**, 182–190.

124 X. Yang and C. Wang, *Chin. J. Chem.*, 2018, **36**, 1047–1051.
125 H. Fischer, *Chem. Rev.*, 2001, **101**, 3581–3610.
126 D. Leifert and A. Studer, *Angew. Chem., Int. Ed.*, 2020, **59**, 74–108.
127 A. Vivien, L. Veyre, R. Mirgalet, C. Camp and C. Thieuleux, *Green Chem.*, 2023, **25**, 7721–7728.
128 Q. Li, S. Huo, L. Meng and X. Li, *Catal. Sci. Technol.*, 2022, **12**, 2649–2658.
129 I. K. Goncharova, S. A. Filatov, A. P. Drozdov, A. A. Tereshchenko, P. A. Knyazev, A. A. Guda, I. P. Beletskaya and A. V. Arzumanyan, *J. Catal.*, 2024, **429**, 115269.
130 R. R. Behera, R. Saha, A. A. Kumar, S. Sethi, N. C. Jana and B. Bagh, *J. Org. Chem.*, 2023, **88**, 8133–8149.
131 W. J. Teo, C. Wang, Y. W. Tan and S. Ge, *Angew. Chem., Int. Ed.*, 2017, **56**, 4328–4332.
132 M. Huang, X. Zhou, Y. Shao, Y. Li, Y. Liu and Z. Ke, *J. Catal.*, 2023, **428**, 115197.
133 T. K. Mukhopadhyay, M. Flores, T. L. Groy and R. J. Trovitch, *Chem. Sci.*, 2018, **9**, 7673–7680.
134 J. R. Carney, B. R. Dillon, L. Campbell and S. P. Thomas, *Angew. Chem., Int. Ed.*, 2018, **57**, 10620–10624.
135 L. Britton, M. Skrodzki, G. S. Nichol, A. P. Dominey, P. Pawluć, J. H. Docherty and S. P. Thomas, *ACS Catal.*, 2021, **11**, 6857–6864.
136 M.-Y. Chen, N. Soulé, A. Zuluaga, A. Frot, A. Vivien, C. Camp, C. Thieuleux, P.-A. Payard and M.-E. L. Perrin, *ACS Catal.*, 2025, **15**, 16840–16850.
137 K. Ganguli, A. Mandal, B. Sarkar and S. Kundu, *Tetrahedron*, 2020, **76**, 131439.
138 V. Yempally, A. Shahbaz, W. Y. Fan, S. T. Madrahimov and A. A. Bengali, *Inorganics*, 2020, **8**, 61.
139 S. Weber, D. Iebed, M. Glatz and K. Kirchner, *Monatsh. Chem.*, 2021, **152**, 635–639.
140 T. F. Cruz, L. F. Veiros and P. T. Gomes, *Inorg. Chem.*, 2021, **61**, 1195–1206.
141 N. Almutairi, S. Vijjamarri and G. Du, *Catalysts*, 2023, **13**, 665.
142 K. Matsubara, T. Mitsuyama, S. Shin, M. Hori, R. Ishikawa and Y. Koga, *Organometallics*, 2021, **40**, 1379–1387.
143 K. Matsubara, K. Ikuta, S. Koga and Y. Koga, *J. Organomet. Chem.*, 2025, **1032**, 123634.
144 A. Reisenhofer, F. Belaj, M. Y. Ibrahim and N. C. Mosch-Zanetti, *Appl. Organomet. Chem.*, 2025, **39**, e70129.
145 O. Martinez-Ferrate, B. Chatterjee, C. Werle and W. Leitner, *Catal. Sci. Technol.*, 2019, **9**, 6370–6378.
146 R. J. Trovitch, *Acc. Chem. Res.*, 2017, **50**, 2842–2852.
147 E. Antico, P. Schlichter, C. Werlé and W. Leitner, *JACS Au*, 2021, **1**, 742–749.
148 T. Gonzalez and J. J. García, *Polyhedron*, 2021, **203**, 115242.
149 R. L. Sweany and J. Halpern, *J. Am. Chem. Soc.*, 1977, **99**, 8335–8337.
150 R. R. Behera, R. Ghosh, S. Panda, S. Khamari and B. Bagh, *Org. Lett.*, 2020, **22**, 3642–3648.
151 S. C. Sousa, S. Realista and B. Royo, *Adv. Synth. Catal.*, 2020, **362**, 2437–2443.
152 S. Chakraborty, A. Das and S. K. Mandal, *Chem. Commun.*, 2021, **57**, 12671–12674.
153 G. Vijaykumar, A. Pariyar, J. Ahmed, B. K. Shaw, D. Adhikari and S. K. Mandal, *Chem. Sci.*, 2018, **9**, 2817–2825.
154 M. Bhunia, S. R. Sahoo, B. K. Shaw, S. Vaidya, A. Pariyar, G. Vijaykumar, D. Adhikari and S. K. Mandal, *Chem. Sci.*, 2019, **10**, 7433–7441.
155 S. Chakraborty, A. Das, J. Ahmed, S. Barman and S. K. Mandal, *Chem. Commun.*, 2020, **56**, 13788–13791.
156 R. Haridasan, *Chem. Commun.*, 2019, **55**, 11868–11871.
157 J. T. Reeves, Z. Tan, M. A. Marsini, Z. S. Han, Y. Xu, D. C. Reeves, H. Lee, B. Z. Lu and C. H. Senanayake, *Adv. Synth. Catal.*, 2013, **355**, 47–52.
158 B. L. Tran, M. Pink and D. J. Mindiola, *Organometallics*, 2009, **28**, 2234–2243.
159 S. Das, B. Wendt, K. Moller, K. Junge and M. Beller, *Angew. Chem., Int. Ed.*, 2012, **51**, 1694–1698.
160 R. R. Behara, S. Panda, R. Ghosh, A. A. Kumar and B. Bagh, *Org. Lett.*, 2022, **24**, 9179–9183.